Composites of $CoFe_2O_4$/Graphene Oxide/Kaolinite for Adsorption of Lead Ion from Aqueous Solution

By:-Yared Daniel Reta

A Thesis Submitted to

The department of Materials Science and Engineering

School of Mechanical, Chemical, and Materials Engineering

Presented in Partial Fulfillment of the Requirement for the Degree of Master's in Materials Science and Engineering

Office of Graduate Studies
Adama Science and Technology University

July 2021

Adama, Ethiopia

Composites of $CoFe_2O_4$/Graphene Oxide/Kaolinite for Adsorption of Lead Ion from Aqueous Solution

By:-Yared Daniel Reta

Advisor: Temesgen Debelo Desissa (Ph.D.)

A Thesis Submitted to

The department of Materials Science and Engineering

School of Mechanical, Chemical, and Materials Engineering

Presented in Partial Fulfillment of the Requirement for the Degree of Master's in Materials Science and Engineering

Office of Graduate Studies

Adama Science and Technology University

July 2021

Adama, Ethiopia

Declaration

I hereby declare that this Master Thesis entitled "**Composites of $mCoFe_2O_4$/Graphene Oxide/Kaolinite for Adsorption of Lead Ion from Aqueous Solution"** is my original work. That is, it has not been submitted for the award of any academic degree, diploma, or certificate in any other university. All sources of materials that are used for this thesis have been duly acknowledged through citation.

_____	_____	_____
Name of the Student	Signature	Date

Recommendation

I/we, the advisor(s) of this thesis, hereby certify that I/we have read the revised version of the thesis entitled Composites of "**$CoFe_2O_4$/Graphene Oxide/Kaolinite for Adsorption of Lead Ion from Aqueous Solution**" prepared under my/our guidance by Yared Daniel submitted in partial fulfillment of the requirements for the degree of Master's of Science in Materials Science and Engineering. Therefore, I/we recommend the submission of a revised version of the thesis to the department following the applicable procedures.

Major Advisor	Signature	Date
Co-Advisor	Signature	Date

Approval Sheet

I/we, the advisors of the thesis entitled "**Composites of $CoFe_2O_4$/Graphene Oxide/Kaolinite for Adsorption of Lead Ion from Aqueous Solution**" and developed by Yared Daniel, hereby certify that the recommendation and suggestions made by the board of examiners are appropriately incorporated into the final version of the thesis.

Major Advisor	Signature	Date
Co-Advisor	Signature	Date

We, the undersigned, members of the Board of Examiners of the thesis by Yared Daniel have read and evaluated the thesis entitled "**Composites of $CoFe_2O_4$/Graphene Oxide/Kaolinite for Adsorption of Lead (II) from Aqueous Solution**" and examined the candidate during the open defense. This is, therefore, to certify that the thesis is accepted for partial fulfillment of the requirement of the degree of Master of Science in Materials Science and Engineering.

Chairperson	Signature	Date
Internal Examiner	Signature	Date
External Examiner	Signature	Date

Finally, approval and acceptance of the thesis are contingent upon submission of its final copy to the Office of Postgraduate Studies (OPGS) through the Department Graduate Council (DGC) and School Graduate Committee (SGC).

Department	Head Signature	Date
School Dean	Signature	Date

Office of Postgraduate Studies,	Dean Signature	Date

Acknowledgment

First and foremost, I would like to thank my supervisor Dr. Temesgen Debelo for his patience, guidance, friendly attitude, sharing of many good ideas. Regardless of his workload, he always makes time to answer questions as well as giving very constructive criticism. My thanks also extend to Mr. Demeke Tesfay, Mr. Henoke Mekonen, and all staff members of the Materials Science and Engineering department. I would like to express my gratitude to Adama Science and Technology University for funding this research project under the number ASTU/SM-R/216/21, Adama, Ethiopia. Last but not least, I would like to thank my whole family and friends who supported me through their inspiration and advice.

Contents

List of Figures

List of Tables

List of Acronyms and Symbols

AAS	Atomic Absorption Spectroscopy
C_e	Equilibrium concentration (mg L^{-1})
C_o	Initial concentration (mg L^{-1})
CF-GO	Cobalt ferrite ($CoFe_2O_4$)/Graphene oxide composite
CF-0.30GO	0.7(Cobalt ferrite ($CoFe_2O_4$))/0.3(Graphene oxide composite)
DH_2O	Distilled water
DTA	Differential Thermogravimetric Analysis
EPA	Environmental Protection Agency
FTIR	Fourier transforms infrared spectroscopy
GCF	0.7($CoFe_2O_4$)/0.3(GO)
GO	Graphene oxides
K_1	Rate constant of Pseudo-first-order kinetics (min^{-1})
K_2	Rate constant of pseudo-second-order kinetics ($g.mg^{-1}.min^{-1}$)
K/CF-GO	Kaolinite/Cobalt ferrite/ Graphene oxide composite
SEM	Scanning Electron Microscopy
q_e	Adsorption capacity at equilibrium (mg g^{-1})
q_t	Adsorption capacity at a time t (mg g^{-1})
TGA	Thermogravimetric analysis
XRD	X-Ray Diffraction

Abstract

Heavy and toxic metals removal from wastewater has never been easy and becoming a major concern for environmental and societal health. Among these heavy metals, lead ion (Pb (II)) is highly toxic and can cause great environmental pollution and health effects. Removal of the Pb (II) from aqueous solutions can be performed by utilizing composite materials. In this work, we established composites from kaolinite (K), $CoFe_2O_4$ (CF), and graphene oxide (GO) for adsorption of the lead ion (Pb (II)). Initially, a composite of CF-GO was synthesized by hydrothermal method using cellulose bio-template extracted from false banana. The weight ratio of GO was varied from 0.20 –0.30, i.e., (1-x) CF/(x)GO (x =0.20, 0.25, 0.30). The sample with x = 0.30, i.e., CF-0.3GO exhibited a better adsorption capacity of about 23.6 mg g^{-1} from the binary composite samples at the initial Pb concentration of 50 mg L^{-1}. Then, the contact time and adsorbent dosage of CF-0.3GO were optimized with the corresponding results of 90 min and 1.2 g L^{-1}, respectively. A ternary composite was formulated from the sample of CF-0.3GO and Kaolinite (K) with the nominal composition of (1-y)K/(y)(CF-0.3GO), where y = 0.30, 0.45, 0.60, and 0.75. Among the ternary composites, the sample with a composition of 0.25K/0.75(CF0-0.3GO) showed the best adsorption capacity of about 4.2 mg g^{-1} at the initial Pb concentration of 10 mg $L^{-1,}$ and this sample was subsequently selected for further studies. The synthesized composites were characterized using powder X-ray diffraction (XRD), Scanning electron microscopy (SEM), Fourier transforms infrared spectroscopy (FTIR), and Differential thermogravimetric analysis (TGA-DTA), respectively, to determine phase purity, the particles morphology, functional groups, and thermal stability of samples. Atomic absorption spectroscopy (AAS) was used to determine the adsorption capacity of samples. The effect of pH ranging from 2–10 was investigated for the present composite. At pH of 4, the adsorption capacity and removal efficiency changed significantly, with the corresponding results of 6.62 mg g^{-1} and 99 %, respectively, and becomes constant. Adsorption kinetics were studied for the composite with the composition of (0.25K/0.75[(CF-0.3GO)]) with a time range from 30–120 min. At around 90 min, an equilibrium was established and the kinetic behavior obeyed the Pseudo-second-order adsorption kinetics. Finally, the synthesized composite was stable for three-round tests towards the Pb(II) removal. Therefore, the results of this study indicate that the composites of $CoFe_2O_4$/Graphene oxide/Kaolinite could be a 0potential candidate for the removal of Pb (II) ions.

Keywords: $CoFe_2O_4$/Graphene oxide/Kaolinite, Adsorption and lead ion.

CHAPTER ONE

1. Introduction

1.1. Background of the Study

Water is the most essential substance for human beings' survival although its pollution by different pollutants or contaminants brings severe threats to the health of the environment and the societies [1]. These contaminants may be released from different sources into water bodies. The growth of civilization, population, and industrialization have led to a steady worsening in the purity of available water resources [2].

Processing industries are the main sources of these pollutants [3], among which toxic heavy metal ions, organic dyes, particulate matter, and so on. Heavy metal ions such as Lead (Pb), Cadmium (Cd), Mercury (Hg), Tin (Sn), Iron (Fe), Manganese (Mn), Copper (Cu), Zinc (Zn), Chromium (Cr), Cobalt (Co), Arsenic (As), and Nickel (Ni) can be released from different processing industries such as mineral mining, metallurgical plating, batteries, and fertilizer plants [4, 5]. Among these different heavy and toxic metal ions Pb, Cd, Hg, and As are highly carcinogenic [6].

Pb (II) is an extremely toxic metal and can cause large-scale environmental pollution and health effects in many parts of the world [7]. Generally, human vulnerability to lead is due to drinking water. According to the Environmental Protection Agency (EPA) the supreme pollutant level goal for lead in drinking water at zero because lead can affect human health even at low exposure amounts [8]. Thus, to live in a clean environment and healthy life, the removal of Lead from water is crucial.

There are several techniques to eliminate or minimize the level of these heavy metals such as ion exchange, chemical precipitation, electrolysis, membrane separation, solvent extraction, and adsorption [9]. Among these methods, adsorption is considered the most effective due to its easy operation, low cost, available adsorption materials, and high efficiency.

For the adsorption process, different adsorbent materials can be utilized. The adsorption materials include: carbon nanotubes (CNTs) [2, 10-12], activated carbon [13-16], clay minerals with good adsorbing and ion exchangeability [4], porous nanomaterials [17, 18] inorganic nanoparticles [19-21], metal oxides [22-25], clay-based nanocomposites [26-28], and graphene oxide [29-31].

Clay materials have a low cost and are most abundant so that they are considered efficient adsorbent materials. For the adsorption of heavy metals most commonly used clay minerals are Kaolinite, Montmorillonite, and Bentonite [32]. To improve the adsorption performance, many researchers used modified clay minerals. For instance, montmorillonite and kaolinite clay minerals are modified with sulphuric acid to eliminate copper from water [33]. These clay minerals do not have magnetic properties that limit the reusability of clays for many cycles of operation [34]. Moreover, for adsorption processes, the surface area and pore structure of the clays suffer from clogging and need to be improved, for instance, by formulating composites with nanoparticles [35]. The reusability issue can be minimized by formulating a composite of clay with magnetic spinel ferrites. Among magnetic spinel ferrites, $CoFe_2O_4$ has excellent physical and chemical stability, high surface area, high saturation magnetization, high coercivity, and strong adsorption capacity [36-38]. However, $CoFe_2O_4$ magnetic particles have agglomeration challenges, which can be minimized by synthesizing the $CoFe_2O_4$ using cellulose template synthesis. Moreover, the addition of grapheme oxide (GO) may increase the surface area of clay and prevent the aggregation of spinel ferrites. [38].

In this work, we synthesized composites from kaolinite clays and cellulose-template Cobalt ferrite ($CoFe_2O_4$)/Graphene oxide (GO) for adsorption of lead ions from an aqueous solution. Cellulose was extracted from the *Ensete ventricosum* (false banana). Then the samples were characterized by using X-ray diffraction (XRD), Fourier Transform–Infrared spectroscopy (FTIR), Scanning electron microscopy (SEM), and thermo-gravimetric analysis-differential thermal analysis (TGA-DTA). The adsorption performance of the synthesized composite materials was determined by Atomic absorption spectroscopy (AAS). Parameters such as contact time, adsorbent dosage, and solution pH on adsorption of Pb (II) were investigated. Adsorption kinetics was also studied to determine the mechanism of adsorption.

1.2. Objectives of the study

1.2.1. General Objective

Synthesis and characterization of composites from kaolinite clay, Cobalt ferrite ($CoFe_2O_4$), and Graphene oxide (GO) for adsorption of lead ions from aqueous solution.

1.2.2. Specific Objectives

1. Synthesizing graphene oxide using improved hummers method and to extract cellulose from false banana
2. Synthesizing cellulose-templated $CoFe_2O_4$-GO (CF-GO) composites using the hydrothermal method
3. Synthesizing composite of kaolinite clay and CF-GO using solution methods, followed by materials characterizations
4. Studying the effects of contact time, adsorbent dosage, and pH of the solution on the adsorption capacity and removal efficiency of the composites using atomic absorption spectroscopy (AAS)
5. Studying the kinetics of adsorption to determine the adsorption mechanism

1.3. Scope of the Study

This study covers the use of false banana byproducts as a raw material for the extraction of cellulose to synthesize cellulose template $CoFe_2O_4$/GO. Graphene oxide was synthesized by improved hummers method using Graphite powder as astarting material. Consequently, formulating ternary composite of $CoFe_2O_4$/GO/Kaolinite using locally collected kaolinite clay. It is more focused on designing efficient magnetic adsorbents for the adsorption of lead ions from an aqueous solution.

1.4. Significance of the Study

In our country, different sectors such as industry, pharmaceutical, and agricultural areas are highly expanded and improved our society's life. Industrial effluents released from the processing industries such as metal plating industries, batteries, tanneries, painting and so can

greatly polluting water bodies. In this work, a simple and efficient method is used for the synthesis of $CoFe_2O_4$/GO/Kaolinite for the adsorption of lead ions from an aqueous solution. Lead ion is highly toxic and carcinogenic due to this it can affect various systems in our body. Therefore, this study will provide effective materials for the elimination of lead ions.

CHAPTER TWO

2. Literature Review

In this section, we reviewed water purification methods, adsorption process, and parameters that affect the adsorption process. In addition to that, various adsorbents (kaolinite clay, metal oxides, clay-based nanocomposites, and graphene oxide) for the removal of heavy metals from wastewater with a special focus on recent papers have also been reviewed.

2.1. Wastewater Purification Techniques

Various techniques have been used to eliminate heavy metal ions from wastewater like chemical precipitation, membrane filtration, ion exchange, chemical coagulation, and flocculation, bioremediation, and adsorption [39]. From these methods, adsorption has been commonly considered as a highly efficient technique for the elimination of heavy metals from wastewater due to its low cost, effective and cheap operation, easy and various designs, and high capacity [40]. Figure 2.1 below illustrates the conventional technology for the removal of heavy metals.

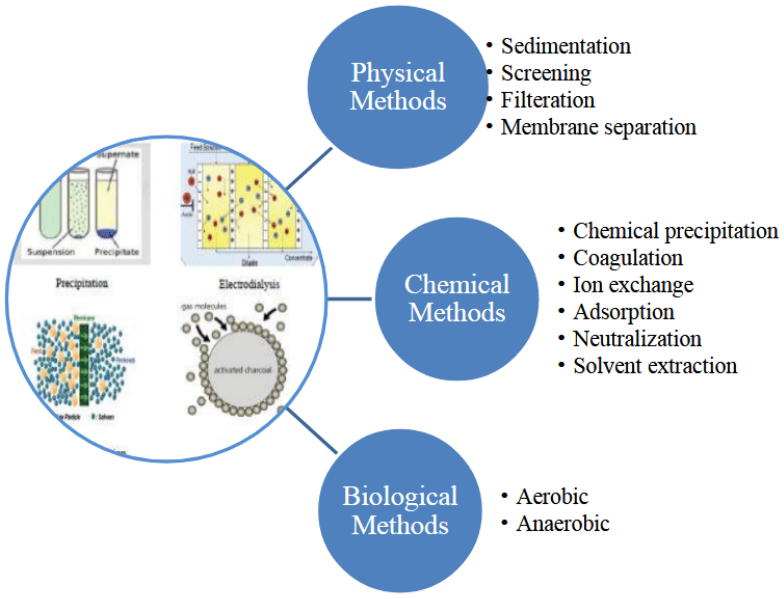

Figure 2.1. Conventional Technology for Heavy Metal Removal [41].

2.2. Adsorption Process

Adsorption is the deposition and adhesion of ions or molecule species onto a surface [42]. It is based on two fundamental parameters; the adsorbent and the adsorbate. The adsorbent is the surface at which ions or molecules are adsorbed whereas; the adsorbate is the species that is adsorbed. The surface where adsorption occurs is provided by the adsorbent and the species adsorbed on the surface is adsorbate (Figure 2.2).

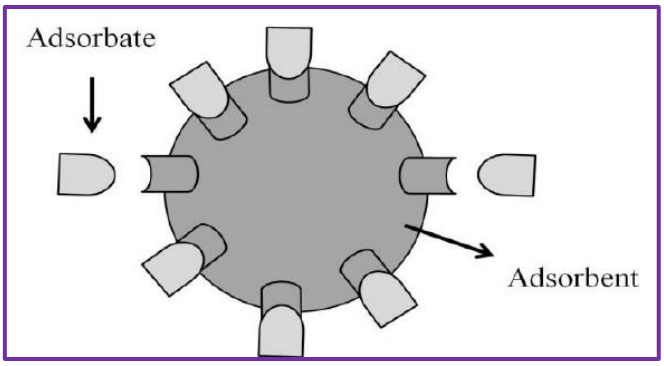

Figure 2.2. Adsorption process scheme adapted from reference [43].

Generally, commercially available adsorbent materials are characterized by high porous structure, porous surface areas ranging from 100 to 1200 $m^2 g^{-1}$. Although low bonding energy is enough to permit the adsorbent to be regenerated by up-taking the adsorbed species, high bonding energy is needed for adsorption to occur [44]. The reverse process is called desorption at which the adsorbed species separated from the surface of the adsorbent to the liquid phase [4]. For this process differences in pH value, temperature and concentration are very important. The adsorbent uptake capacity depends on the adsorption properties such as porosity, specific surface area, pore-volume, cation exchange capacity, interaction time, and adsorbent dose.

Adsorption is the most commonly used method for wastewater treatment due to its ease of operation and availability, cost-effectiveness, and easy handling [4]. However, the adsorption process has its drawbacks such as the absence of accessible adsorbents with high removal capacity for very few metal ion concentrations and a certain adsorbent cannot be used for all contaminants. Physiochemical parameters can affect the removal efficiency using adsorbents such as pH, temperature, contact time, adsorbent dose, initial pollutants concentration, etc. [45].

2.3. Parameters Affecting Adsorption Process

2.3.1. Contact Time

Various parameters influence the adsorption process, among those parameters contact time has a significant effect on the adsorption [46]. As the contact time increased the adsorption rate of clay minerals also increases, then after the equilibrium time was obtained and the rate will be constant. Physical and chemical properties can seriously affect the contact time for the adsorption of heavy metals in the wastewater. Mostafa R. et al., [45] studied the Kaolinite nanotubes (KNTs) for adsorption of Zn (II), Cd (II), Pb (II), and Cr (VI) as exhibited in Figure 2.3. In their study, KNTs was exhibited a longer equilibrium time. For instance, the equilibration time of Cd (II) and Pb (II) adsorption was 360 min which suggesting that various kinds of functional groups require enough time with the adsorbed metal ions to be saturated.

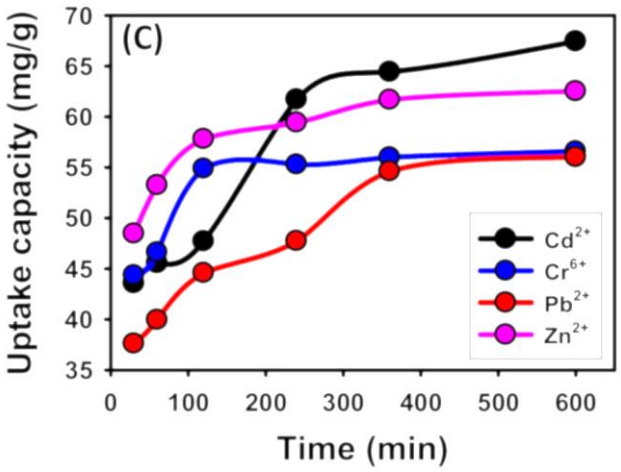

Figure 2.3. Effect of contact time on the adsorption properties of KNTs for Zn (II), Cd (II), Pb (II), and Cr (VI) ions [45].

Based on other parameters such as clay mineral composition, heavy metal type and pH of the system, complete removal of heavy metals could take place up to 6 hours [42]. These parameters are also responsible for a long period of water treatment. For instance, one research observed that adsorption of heavy metal did not take place in the first 21 days of the experiment, whereas after 111 days 75% of heavy metals were removed [47]. The high amount of active sites on the adsorbent and high concentration of heavy metals could improve the rate of adsorption. However, as the time is further increased, the rate of adsorption is slow down due to the reduction of available active sites that were filled with heavy metal ions [4, 42]. If the reaction is left to goes on, the heavy metal cations begin to move from the outer to the inner sites of the clay minerals, resulting in a slower removal rate. Adsorption efficiency increases for Cd (II) from 39.12 to 52.31%, for Cu (II) 31.24 to 82.13%, for Ni (II) 13.13 to 27.36% and Zn (II) is 10.26 to 40.74% as the contact time increases from 15 to 240 min [48]. The obtained result suggested that the uptake capacity is higher during the initial stage due to the availability of a large number of active sites on the adsorbent. At 45 min of stirring time, the maximum removal was obtained and after 180 min, no change in the adsorption efficiency due to the occupation of the active site by the metal ions.

The contact time for the adsorption process was lesser in comparison to the heavy metal adsorption process by polyaniline nanocomposite material [49]. It was also observed that

physical and chemical properties affect the contact time for the adsorption of heavy metals present in the water.

2.3.2. pH of the Solution

The pH value plays a crucial role in the adsorption process. Various researchers studied the effect of pH on adsorption capacity. Some of these studies are presented in this section. The adsorption of Pb (II), Cd II), Ni (II), and Cu (II) in an aqueous solution on raw kaolinite clay was investigated [50]. The solution pH showed a serious impact on the adsorption of metal ions onto kaolinite clay. As pH of solutions increased, the adsorption of Pb (II), Cd (II), Ni (II), and Cu (II) was also increased, for instance, 98% Pb (II) at pH of 6.0, 98% Cu (II) at pH of 6.5 can be removed. This is due to the surface of the kaolinite clay become more negatively charged and containing a large number of active sites, which enhances the adsorption of the positively charged metal ions over an electrostatic force of attraction.

Ajay Kumar et al., studied the biosorption of heavy metals on activated sludge [48]. They suggested that at low pH metal uptake was less and this is because cell walls are closely associated with HO groups and access of metal ions to cell walls would be restricted as a result of repulsive forces. Metal uptake increased with pH from 3-4, which could be associated with ligands with the negative charge being exposed with the subsequent increase in attraction sites to positively charged metal ions. Beyond this point, there is not much further increase in efficiency until pH 6. After pH 6, the efficiency of the bio-sorption process increased drastically due to the formation of metal hydroxides with their respective metal ions. This is mostly due to the metal precipitation as hydroxides which depend on the pH and ion concentration but not due to the biosorption. It was initially thought that, at higher pH values, metals may accumulate inside the cells or cell walls by a mechanism known as combined sorption-micro precipitation. The adsorption of Cd (II) ions on natural clay were studied by the influence of pH value [51]. Figure 2.4 shows the removal efficiency of Cd (II) ions using natural clay as a function of pH.

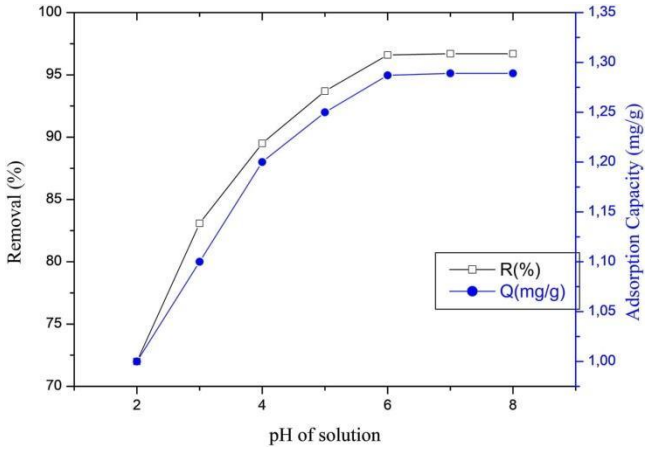

Figure 2.4. pH effect of the adsorption of Cd (II) ions [51].

Southichak, B., et al., investigated the biomass of reed consisting of leaves as a biosorbent for Cu (II), Cd (II), Ni (II), Pb (II), and Zn (II) removal from aqueous solutions [52]. The effect of solution pH upon Cu (II), Cd (II), Ni(II), Pb (II), and Zn (II) removal by reed biomass treated with NaOH (RTN) together with its relation to the electrical charge was studied. Initially, the pH for 12 h of the adsorption experiments was only 0.2. The maximum adsorption of Pb (II) was observed from pH 4, Cu (II) from pH 5, Ni (II) from pH 6, and Zn (II) and Cd (II) from pH 7. The percentage of heavy metal removal by reed biosorbent at the optimum pH was over 80% for all heavy metals. At pH higher than 8, the higher removal efficiency of heavy metal could be obtained due to the precipitation phenomenon. They suggested that no precipitation of heavy metal was observed in this study probably due to the low concentration of heavy metal used.

The conducting polymer, polypyrrole, Polyaniline, coal fly ash, mixed metal oxide, titanium oxide, zinc oxide, and aluminum oxide have been utilized to remove heavy metals from wastewater in the pH range from 2-8 [49]. Based on the obtained result at high pH, a high adsorption rate of heavy metals was observed. The adsorption characteristic of carbon nanotubes is also affected by the concentration of metal concentrations and pH values. The highest removal of metal ions from the water medium is observed between the pH value of 6-8 by the polymeric materials and a value of 4 might be effective for Cr (VI) removal at room temperature.

2.3.3. Temperature of the Solution

Temperature plays a major role in the adsorption of heavy metals. Generally, as the temperature increases, the rate of adsorbate diffusion across the external boundary layer also increased in the internal pores of the adsorbate particles due to liquid viscosity decreases [48]. In addition to that, it also affects the equilibrium capacity of the adsorbate depending on whether the process is exothermic and endothermic. Figure 2.5 illustrates the relationship between the adsorption capacity and temperature for two different materials systems, i.e., activated carbon and $CoFe_2O_4$ towards Cr (VI) removal.

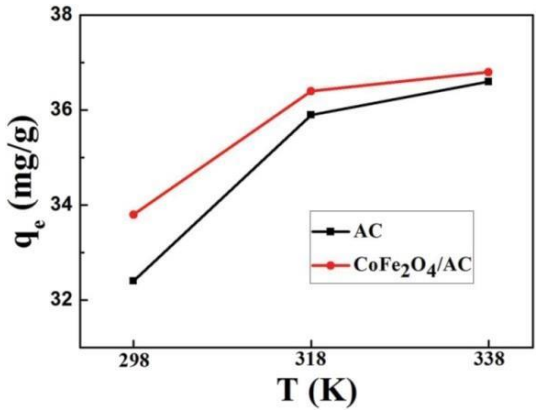

Figure 2.5. Effect of temperature on Cr (VI) adsorption of activated carbon (AC) and $CoFe_2O_4$/AC (the initial Cr (VI) concentration of 150 mg L-1 and pH = 2.0)[53].

As a whole, it is seen that as the temperature increases the loading capacity for the same initial adsorbate concentration decreases. This means that the rate of desorption was more significant than the rate of adsorption, which implies that adsorption is an exothermic reaction. S. Mustapha et al., [54] were studied raw and beneficiated kaolin to remove heavy metals (Cr (VI), Cd (II), and Zn (II)) from tannery wastewater was studied. They observed that, as temperature increases, the removal ability of kaolin was also increased; this showed that, the adsorptive property was also temperature-dependent.

2.3.4. Dosage of Adsorbent

The adsorbent dosage is an important factor in controlling the adsorption rates. At present, there are no specific guidelines on the recommended dosage for efficient adsorption, but it has been established that a small dosage of adsorbent is enough to adsorb a reasonable

concentration of heavy metals from contaminated media [49]. As adsorbent dosage on the biosorption of various increases metal ions, the removal efficiency increases as the sludge mass increases due to the increase of binding sites [55]. After some point, sorption capacity was steady or decreased with biomass concentration due to a screen effect between cells; this produced a block of the cell active sites by an increase of biomass in the system. Removal efficiency increases for Cd (II) from 37.61 to 61.11 %, for Cu (II) 23.36 to 50.28 %, for Ni (II) 12.04 to 27.54 % and Zn (II) is 9.2 to 36.28 % as the mass increases from 0.5g to 3g\(Figure 2.6) [48]. This difference in adsorption shows that the adsorbent has more affinities towards Cd (II) than Cu (II), (Ni (II), and Zn (II) respectively.

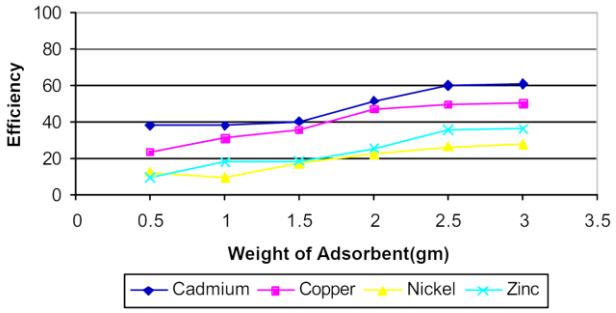

Figure 2.6. Effect of adsorbent dosage on the adsorption capacities and percentage removal efficiencies of Cu(II) and Ni(II) ions by raw kaolinite and acid-activated kaolinite at pH of 7.0, contact time of 60 min, and solution temperature of 25 °C [48].

2.3.5. Specific Surface Area (SSA) of the Adsorbent

The rate of adsorption directly depends on the surface area of the adsorbent, that is, the larger the surface area of the adsorbent, the high efficiency of adsorption [56]. The surface area of a solid powder adsorbent depends on the size of its particles. Various nanostructured carbon-based materials such as carbon nanotubes (CNTs), graphene, carbon fibers, etc. are well known for their extraordinary adsorption properties [4]. Among these carbon materials, CNTs are one of the favorable materials as they have a specific surface area of around 950 $m^2 g^{-1}$. Figure 2.7 shows the effect of the SSA of bio-char and the adsorption capacity against different heavy metals [57]. For chromium, zinc, and lead, a direct relation was observed between surface area and adsorption capacity whereas a positive correlation could not be observed for copper and cadmium.

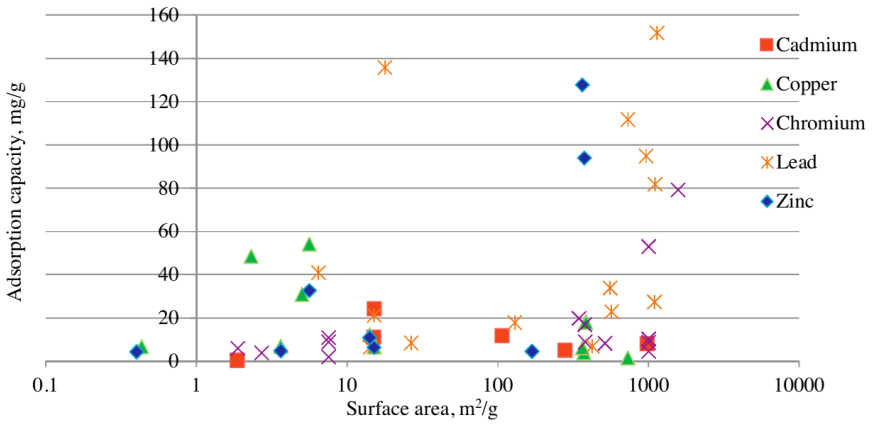

Figure 2.7. The effect of surface area on adsorption capacity of biochar to adsorb selected heavy metals [57].

2.4. Clay Minerals for Adsorption

Clays are layers of aluminosilicates composed of mixtures of fine-grained clay minerals, crystals of other minerals, and metal oxides [58]. Clays have various physical properties such as plasticity, shrinkage under fire and air drying, fineness of grain, color after firing, hardness, cohesion, etc. Physical properties depend on different parameters that control the behavioral pattern of the material. Porosity, saturation, pore fluid conductivity, water content, and clay content are important for electrical conductivity. Sedimentation properties of clay depending upon porosity, water content, and minerals content of different specific gravity [59].

2.4.1. Structure of Common Clay Minerals

Most of the clay minerals are mainly composed of layers containing silica and alumina sheets, which belong to the class of layer silicates group [60]. These groups can be subdivided according to the type of layer structure. Clays consist of an interconnected silicates sheet combined with a second sheet-like grouping of metallic atoms, oxygen, and hydroxyl. The 1:1 clay minerals type consists of one tetrahedral sheet (Figure 2.8), one octahedral sheet (Fig. 2.9), layers, and interlayer minerals, which are explained as follows.

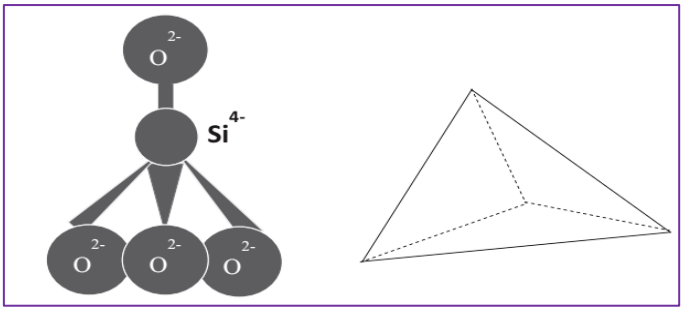

Figure 2.8. Silica sheets consist of $(SiO_4)^{4-}$ tetrahedra connected at three corners [58].

A. Tetrahedral Sheet

Si (IV) cation is the dominant atom in the tetrahedron sheets; however, Al (III) cation can also happen at this site [59]. Substitution of A1(III) for Si (IV) produces an insufficient charge that should be balanced in the structure This $(SiO_4)^{-4}$ tetrahedron is the basic structural unit of all silicate minerals. The Si–O bond is said to be a 50% ionic bond. The bond angle between each Si–O bond in the tetrahedron is 109.5°.

B. Octahedral Sheet

Different phyllosilicate has not had the same cations in the octahedral [59]. High-charged phyllosilicates (example, A1(III)) with relatively in the octahedra, it is necessary that for every two octahedra that contain A1(III), there is an empty octahedron.

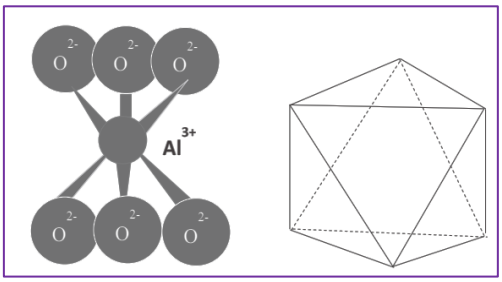

Figure 2.9. Octahedron consists of central cation (Al (III), Fe (II), Mg (II)) surrounded by 6 oxygen (or hydroxyls)[58].

C. Layers

The tetrahedral and octahedral sheets are expansible parts of a phyllosilicate [60]. Thus these two sheets must be connected. The lateral dimensions of the two sheets are approximately equal so it is possible to join them together.

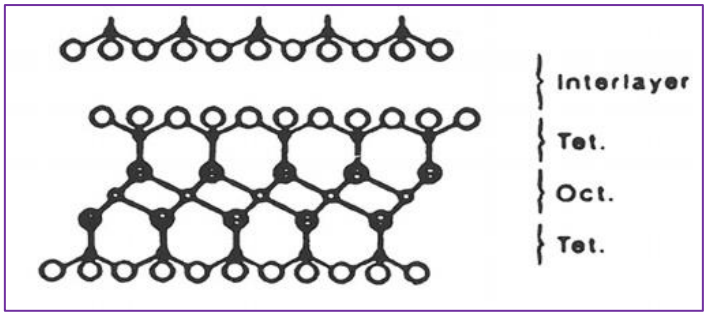

Figure 2.10. A layer structural side views. The octahedral sheet is sandwiched between two opposing tetrahedral sheets. Adapted from reference[60]

The tetrahedral linkages form the tetrahedral sheet, it takes less oxygen to complete the linkage than if we had two individual sheets because there is a common junction between the two. This common junction is a plane of oxygen and hydroxyls that belongs to both the tetrahedral sheet and the octahedral sheet (Figure 2.10).

D. Interlayer Materials

Cations such as Na (I), K (I), Ca (II), or Mg (II) are easy to enter into the interlayer [60]. Depending on the nature of the cation, polar H_2O molecules can also place on the interlayer. For instance, copious amounts of H_2O flow into the interlayer with Na, whereas many fewer H_2O molecules enter the interlayer with Ca (II). As long as there is a huge amount of that material in the environment, there is an easy way to replace interlayer cations with other materials. For instance, a solution of water including Na (I) on every side of a montmorillonite grain will be willingly permitted for Na (I) to interchange for K (I). Hence, these cations are frequently said to be exchangeable cations.

2.4.2. Structure of Kaolinite Clay

Kaolin is a sedimentary rock that is characterized by lightweight and chalk-like features. The principal compositions of kaolin are quartz and mica it also consists of other minerals such as feldspar, montmorillonite illite, ilmenite, haematite, anatase, rutile, kyanite, zircon, graphite, and attapulgite, etc. in an extremely little quantity [61]. Kaolinite clay composed an alternative SiO_4 tetrahedral Al (O, OH) $_6$ octahedral sheets. It has a 1:1 layer structure, Figure 2.11, and plate-like morphology.

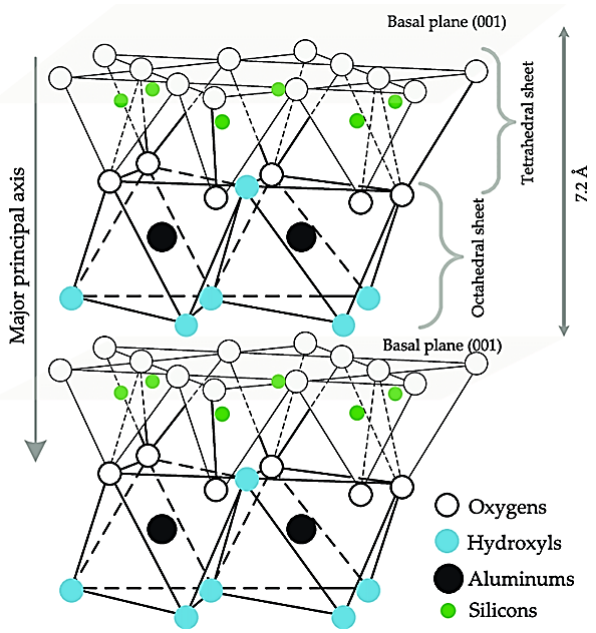

Figure 2.11. Diagrammatic representation of kaolinite structure [62]

Kaolinite is a type of clay that is mainly formed by the kaolinization process by the decomposition of potassium feldspars, granite, and aluminum silicates [61]. It has white or greyish-white color. The melting point of kaolinite clay is about 1750 °C. Kaolinite crystal system is triclinic which has space group P1, in addition lattice parameters are a = 0.515 nm, b = 0.895 nm, c = 0,740 nm, α = 91.68°, β = 104.87°, γ = 89.9°. Its crystal-chemical formula is $Al_4Si_4O_{10}$ $(OH)_8$. Its molecular formula is $Al_2Si_2O_5$ $(OH)_4$, which contains 39, 8 % alumina, 46, 3 % silica, and 13,9 % water which represents a two-layer crystal (silicon-oxygen tetrahedral layer joined to alumina octahedral layer exist alternately). The molecular weight of the structure is -258,071 g mol^{-1}. Kaolinite density is 2.6 g $(cm^3)^{-1}$. The thermal stability of kaolinite is highly dependent on the density of defects. The lower density of defects sample is more stable whereas at high temperatures the dehydroxylation starts.

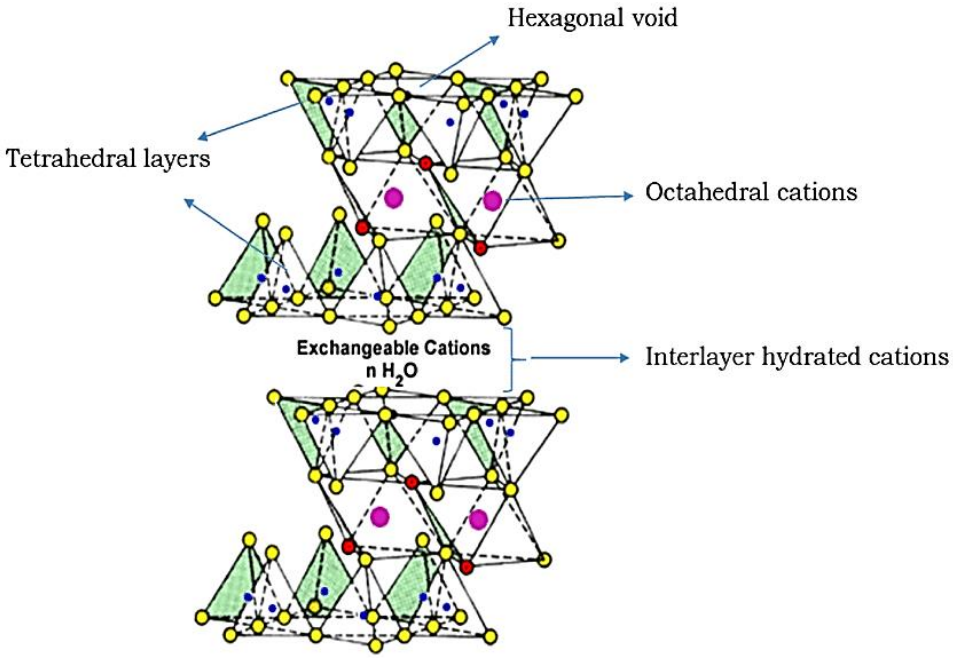

Figure 2.12. Model diagram of montmorillonite clay structure[63].

2.4.3. Montmorillonites (Smectite) Clay Structure

Montmorillonites (Smectite) consist of an octahedral alumina sheet between two rival tetrahedral silica sheets and which have a 2:1 layer structure as exhibited in Figure 2.12. Some of the oxygen exists on both tetrahedral sheets as well as an octahedral sheet. In addition to that, it has weak bonding between two tetrahedral sheets, water, and exchangeable ions easily entered between sheets. This is the main reason for the evolution of swelling capacity. Bentonite clay consists of both the crystalline structure of montmorillonite and other additional crystalline structures like quartz, volcanic glass, feldspar, organic matter, gypsum, etc. [64]. Montmorillonite is the main component of bentonite (70–95%). In tetrahedral substitution of cations occurred. When exchangeable interlayer cations (Na (I), Ca (II), Mg (II), etc.) are introduced layer charge is compensated [65]. The inner and outer surface of the crystal, active sites will be provided. These individualities of montmorillonite structure indicate particular properties of bentonite clays, mainly high adsorption ability towards heavy metals.

2.4.4. Commonly Used Clay Materials for Adsorption

To enhance the adsorption properties like specific surface area, surface functional group, pore volume and size, cation exchange capacity, etc., many researchers have used modified clay minerals by treating them with various chemicals [4]. Kaolinite, montmorillonite, and bentonite are commonly used clay minerals due to their high specific area, availability, stability and structural characteristics, and nontoxicity [4, 54]. In this section commonly used clay minerals (kaolinite, montmorillonite, and bentonite) for heavy metal removals by using in their raw and modified forms have been conferred. Here common clay minerals used in the raw and modified form for the removal of heavy metal pollutants with their results are reviewed by focusing on the most recent researches.

2.4.4.1. Kaolinite

Kaolinite is a hydrous aluminum silicate that has a stable chemical structure and superior physical properties for the production of ceramics. Several researchers have used raw kaolinite and modified kaolinite to investigate the uptake capacity of various heavy metal ions from water solutions. The adsorption of Pb(II) ions onto natural kaolinite clay from water kaolinite was estimated by Jiang et al., [50]. The adsorption of Pb (II), Cd (II), Ni (II), and Cu (II) in an aqueous solution on raw kaolinite clay was investigated through some physicochemical parameters (with variable concentration of metal ion, amount of clay, pH, and mixing time. However, the solution pH showed a serious impact on the adsorption of metal ions onto kaolinite clay. As pH of solutions increased, the adsorption of Pb (II), Cd (II), Ni (II), and Cu (II) was also increased, for instance, 98% Pb (II) at pH of 6.0, 98% Cu (II) at pH of 6.5 can be removed. This is due to the surface of the kaolinite clay become more negatively charged and containing a large number of active sites, which enhances the adsorption of the positively charged metal ions over the electrostatic force of attraction [66]. Kaolinite clay was utilized for up-taking metal ions from wastewater like Pb (II), where its composition was decreased from 160.0 to 8.0 mg L^{-1}.

S. Mustapha et al., [54] used the raw and beneficiated kaolin to remove heavy metals (sulfate, chromium, cadmium, and zinc) from tannery wastewater. The beneficiated kaolin sample was used to remove the unwanted mineral to improve the adsorption capacity of raw kaolin. The

beneficiation process was done by the wet/soaking method. The beneficiated kaolin showed a reduction of Fe percentage and the existence of K in the raw kaolin. These results suggested that there is a tendency of cations exchange between exchangeable cations in the kaolin samples and metal ions in solution, these enhancing adsorption and removal capacity of the metal ion by the kaolinite samples. As temperature increases the removal ability of kaolin was also increased, this showed that adsorptive properties were also temperature-dependent. From this, we can understand that beneficiated kaolin is an effective and low-cost adsorbent to remove contaminants from tannery wastewater.

Mostafa R. et al., [45] synthesized the Kaolinite nanotubes (KNTs) from the raw kaolinite by the method of ultrasonic scrolling for adsorption of Zn (II), Cd (II), Pb (II), and Cr (VI). This conversion enhanced the pore volume and surface area in comparison with the raw kaolinite. By using these KNTs for Cd (II), Zn (II), Cr (VI), and Pb (II) they obtained removal capacity of 116 mg g^{-1}, 103 mg g^{-1}, 91 mg g^{-1}, and 89 mg g^{-1} respectively. These values are higher than various kaolinite and CNTs based adsorbents. In this study KNTs exhibit longer equilibrium time, for instance, the equilibration time of Cd (II) and Pb (II) adsorption was 360 min, these suggested that various kinds of functional groups need enough time with the adsorbed metal ions to be saturated, and also there is an existence of high adsorption sites on the surface of KNTs. Recyclability of these KNTs is also possible. It can be used about five times for the removal of heavy metal ions; however, the percentage of removal is decreased by a certain amount during repeating. So that, modification of kaolinite sheet into KNTs could provide outstanding adsorption properties. This paper also suggested that the adsorption ability of KNTs than that of CNTs consequently, KNTs with different modifications could provide better adsorption properties as well as can be used practically for tap, ground, and sewage water from several contaminants.

Lertcumfu, N., et al., [67] investigated the adsorption properties of composite by the additive of graphene oxide onto a kaolin-based geopolymer. Geopolymers are inorganic polymers that can synthesize by the chemical reaction between an alkaline solution and aluminosilicate minerals (kaolin in this case). They were synthesized graphene oxide by Hummer's method. They modified the raw kaolin into metakaolin (MK) by heating the kaolin at 750 °C for 3 h. then they produced the composite precursor via the geo-polymerization process. The impact of

adding grapheme oxide (0–10 wt. %) to the geopolymer on the adsorptive properties was also investigated. From the adsorption study, the addition of graphene oxide enhanced the uptake capacity i.e., 65 % at 10 wt. % of GO for Cr (VI) after adsorption equilibrium is achieved. This is due to the high surface area and several oxygen functional groups like hydroxyl and carboxyl groups of graphene oxide. Consequently, the GP-GO composite has the capability for wastewater remediation applications.

2.4.4.2. Montmorillonite

Montmorillonite clay is used for adsorption by various researchers in raw or modified form. By focusing on the current researches this section tries to review some papers related to this area. Adsorption of arsenate and arsenite from aqueous solutions using Ti pillared montmorillonite (Ti-MMT) was studied [68] by varying such parameters as contact time, pH, and temperature. The obtained result suggested that adsorption of both arsenate and arsenite were temperature and pH-dependent and also it was noticed that Ti-pillared montmorillonite is an effective adsorbent material for the elimination of these heavy metal ions**.**

Ghorbanzadeh et al., [69] also investigated the removal of arsenate and arsenite by adsorption on montmorillonite in streams media. They obtained adsorption rates of 99.5% for arsenate and 68.2% for arsenite, based on that they stated that this clay mineral is an efficient adsorbent for heavy metals. Montmorillonite clay utilized as an efficient adsorbent to adsorb La and Yb species was investigated by Alshameri et al. [70].

N.D. Mu'azu et al., [82] were studied the effect of montmorillonite with different content in a natural clay mineral on the sorption properties for the removal of Cu (II) and Ni (II) from water. To investigate this they used various physiochemical parameters such as contact time, the mass of adsorbent, pH, and initial metal concentration. The composition of clay was mainly kaolinite and muscovite with a small amount of quartz, whereas the bentonite was contained a high amount of montmorillonite with a surface area of 20.83 and 44.27 m^2 g^{-1} respectively. As the content of montmorillonite content increased in the clay the uptake capacity for Ni (II) adsorption was increased whereas decreased for Cu (II) removal. Montmorillonite content was also showed a series effect on the equilibrium time. As this content increased the time was also increased and a higher equilibrium time was obtained for

the case of natural clay than the bentonite. The optimum uptake capacity for Cu (II) and Ni (II) was 16.38 and 8.66 mg g^{-1} respectively. The obtained results indicated that the utilization of various mineralogical components in clay adsorbents is can influence the sorption of heavy metal ions from water as well as the composition of montmorillonite content in clay highly to control different metal ions removal from aqueous solution.

2.4.4.3. Bentonite

Bentonite clay in raw and modified form is studied by various researchers. D. Kurnosov et al., [71] produced modified bentonite clay by multiwall carbon nanotubes (MWCNTs) to obtain efficient adsorption material. This composite material was produced by immersing the raw clay with a catalyst solution subsequently by heat treatment. The MWCNTs were synthesized by chemical vapor deposition (CVD) under pilot production conditions. The removal capacity of the modified nano adsorbent was studied in comparison with the raw bentonite. The nanocomposite can be reduced the equilibrium adsorption time than that of the natural bentonite i.e. the nano adsorbent is saturated within 100-300 min; while in the case of the raw adsorbent saturated time was 400-1200 min. This suggested that modification of the structure of the bentonite clay with the MWCNTs could enhance the uptake capacity and reduce the equilibrium times for the removal of heavy metals.

S. Kakaei et al., [72] investigated bentonite clay was modified with imidazole and imidazolium groups for the removal of Co (II), Cu (II, and Pb (II). They observed the modification of bentonite by imidazole could enhance the uptake of heavy metals from wastewater. Table 2.1 summarizes the adsorption of heavy metal ions by using clay-based materials.

Table 2. 1. Application of clay-based materials for the removal of heavy metal ions.

S/N	Raw materials	Modifying agent	Type of metal(s) removed	Adsorption capacity in (mg/g)	Ref.
	Kaolinite nanotubes(KNTs)		Zinc(II) Cadmium(II) Lead(II) Chromium(VI)	103 116 89 91	[73]
1.	Kaolinite	Hydrochloric acid Acetic acid	Chromium(VI) Iron(III) Chromium(VI) Iron(III)	18.15 39.80 10.42 19.34	[74]
2.	Kaolinite	Zirconium oxychloride	Iron(III) Cobalt(II) Nickel(II)	9.7 9.6 8.8	[75]
3.	Kaolinite	Raw Manganese oxide	Cadmium(II) Cadmium(II)	14.11 36.47	[76]
4.	Kaolinite	Raw Sodium tetraborate Raw Sodium tetraborate	Lead(II) Lead(II) Cadmium(II) Cadmium(II)	16.16 42.92 10.75 44.05	[77]
5.	Montmorillonite	Zirconium oxychloride	Iron(III) Cobalt(II) Nickel(II)	23.8 22.8 22.0	[75]
6.	Montmorillonite	Raw Histidine Raw Histidine	Lead(II) Lead(II) Copper(II) Copper(II)	89.08 23.93 107.73 30.72	[78]
7.	Montmorillonite	Tourmaline	Lead(II)	303.21	[79]
	Bentonite	Bencylhexadecyldimethyl ammonium chloride	Copper(II) Zinc(II)	50.76 35.21	[80]

From the kinetics study, the modified bentonite by imidazole showed higher uptake capacity and adsorption efficiency in comparison with the raw bentonite and modified bentonite by imidazolium. It is indicated that at pH 5 the highest amount of metal was adsorbed. The adsorption efficiency was also higher in the case of modified bentonite by imidazoline.

R.R. Pawar et al., [81] studied the uptake of toxic heavy metal ions i.e. Cu (II) and Pb (II) by fabricating activated bentonite-alginate (ABn-AG) composite beads. ABn-AG was produced by the ionic gelation method. At higher acidic conditions 58% of Cu (II) and 77% of Pb (II)

were detached at pH 2. The optimum sorption capacity for Cu (II) and Pb (II) was about 17.3 mg g^{-1} and 107.52 mg g^{-1} respectively. The presence of various sites in the ABn-AG composite allows the adsorption of both Cu (II) and Pb (II). The removal efficiency of Cu (II) and Pb(II) was decreased only by 10% during the reusability test; these suggested that reusing of ABn-AG is practicable with a negligible decrease in uptake ability. After using these composite beads for the application of adsorption separation and recovery were also possible by varying some physicochemical parameters.

Although the existence of background electrolytes like $CaCl_2$, $MgCl_2$, NaCl, and KCl did not cause serious influence on the sorption of Pb (II), Cu (II) removal was constrained by the presence of $CaCl_2$. Consequently, their investigation indicated that ABn-AG composite beads could be employed as an effective and economical adsorbent for the uptake of Cu (II) and Pb (II) from wastewater.

2.5. Spinel Structured Ferrites (MF_2O_4)

Spinel ferrites with MFe_2O_4 formula (M = Fe (II), Mn (II), Co (II), Zn (II), etc.) are a group of metal magnetic nanoparticles. These materials are widely used as efficient adsorbent materials to remove heavy metal ions due to their magnetic features and easy separation [1]. Figure 2.13 shows the schematic unit cell structure of $CoFe_2O_4$.

Many researchers focused on spinel ferrites due to their outstanding properties, some of the researches are presented in this section. The removal of zinc from an aqueous medium was investigated by using $MnFe_2O_4$ and $CoFe_2O_4$ spinel ferrites nanoparticles. $MnFe_2O_4$ and $CoFe_2O_4$ spinel ferrites were synthesized by the co-precipitation method. The effects of initial pH, contact time, metal ion concentration, and temperature on Zn (II) adsorption were also studied. The maximum adsorption capacity was 454.5 and 384.6 mg g^{-1} for $MnFe_2O_4$ and $CoFe_2O_4$ at pH 6 respectively. Also, the reusability and the desorption capability of adsorbents were investigated [1].

The adsorption capacity of different MFe_2O_4 (M=Mn, Fe, Co, Ni) ferrite nanocrystals was compared. The nanoparticles were synthesized by the hydrothermal method. They suggested that the distribution of MFe_2O_4 cations of ferrites is the most essential factor for adsorption

capacity. The ferromagnetic behavior of MFe_2O_4 nanoparticles allowed the high-efficient magnetic separation from wastewater. Based on the result, $CoFe_2O_4$ nanocrystals exhibit a higher saturation magnetization of 86.1emu g^{-1} as well as outstanding adsorption capacity. The obtained result showed the maximum adsorption capacity of $CoFe_2O_4$ for CR is 244.5 mg g^{-1}.

Santhosh C., et al., synthesized magnetic cobalt and nickel ferrites ($CoFe_2O_4$ & $NiFe_2O_4$) with graphene nanocomposites ($CoFe_2O_4$–G & $NiFe_2O_4$–G) via a solvothermal process [38]. The composite was used as an adsorbent for the removal of lead and cadmium ions from an aqueous solution. The effect of various parameters like contact time, adsorbent dose, solution pH, and temperature was studied. The maximum adsorption equilibrium for the Pb(II) was about 142 and 111mg g^{-1} at pH of 5 for $CoFe_2O_4$–G & $NiFe_2O_4$–G respectively. Whereas for Cd (II) it was about 105 and 74 mg g^{-1} at a pH of 7. Based on the obtained result, they suggested that this material can be used for efficient adsorption.

Vazquez-Olmos, A.R., et al., [82] investigated the adsorption of Pb(II) from aqueous solution by using MFe_2O_4 nanoparticles (M = Co, Ni, and Zn). Nanoferrite samples were prepared via the mechanochemical method and were used for the preparation of nano ferrites. At room temperature, $NiFe_2O_4$ and $ZnFe_2O_4$ samples showed superparamagnetic behavior. Table 2.2 shows some applications of MFe_2O_4 for the adsorption of heavy metal ions.

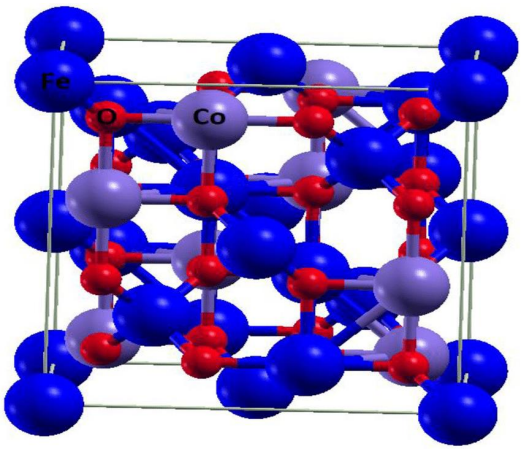

Figure 2.13. The unit cell structure of cobalt ferrite ($CoFe_2O_4$) [83]

Table 2. 2. Application of MFe_2O_4 for adsorption of heavy metal ions.

S/N	Raw materials	Modifying agent	Type of metal(s) removed	Adsorption capacity in (mg/g)	Ref.
1.	$MnFe_2O_4$ $CoFe_2O_4$		Zinc(VI) Zinc(VI)	454.5 384.6	[1]
2.	$CoFe_2O_4$ Fe_2O_3 Co_3O_4		Lead(III)	326.79 140.84 284.90	[84]
3.	$CoFe_2O_4$	Chitosan	Cadmium(II) Lead(II)	71.53 151.06	[85]
4.	bentonite/$CoFe_2O_4$	MnO_2	Cadmium(II)	115.79	[86]
5.	$CoFe_2O_4$	Cetyltrimethylammonium bromide	Lead(II)	32.11	[87]
6.	$MnFe_2O_4$	Chitosan	Copper(II) Chromium(III)	22.6 15.4	[88]
7.	TEPA-GO/$MnFe_2O_4$	Carbon	Lead(II)	263.2	[89]
8.	neem leaves/$MnFe_2O_4$	Corynebacterium glutamicum	Arsenic(III) Arsenic(V)	343.54 550.67	[90]
9.	$ZnFe_2O_4$	NH_2-SiO_2	Lead(II)	267.2	[91]
10.	Ce^{3+} doped $ZnFe_2O_4$		Chromium(VI)	57.24	[92]
11.	Bentonite/$CoFe_2O_4$/ Hydroxyapatite		Lead(II)	67.1	[93]

2.6. Clay-Based Nanocomposites for Adsorption

Nano-composites materials are formed by the nanoscale dispersion of nanoparticles in matrix-like clay to improve the material properties [4]. Clay-based nanocomposites offer good advantages such as high ion sorption capacity, high specific surface area, low cost, and chemical stability. Various researchers focused on clay-based nanocomposites for the removal of different heavy metals from water and they found that the adsorption efficiency is influenced by several parameters such as dosage of adsorbent, pH, temperature, and initial concentration, etc.

Hydroxyapatite-bentonite clay nanocellulose (CHA-BENT-NCC) composite material was synthesized as an efficient adsorbent for the removal of Ni (II), Cd (II), and $(PO_4)^{-3}$ from aqueous solutions [94]. The effect of pH, contact time, temperature, and initial adsorbate concentration were studied to improve the removal capacity. The maximum adsorption capacity for Ni (II), Cd (II), and $(PO_4)^{3-}$ was estimated to be 29.46 mmol g^{-1}, 10.34 mmol g^{-1}, and 4.90 mmol g^{-1}, respectively. Five adsorption-desorption cycles were performed without a significant decrease in adsorption capacities. The obtained result suggested that CHA-BENT-NCC material is a very effective adsorption material for the treatment of mining water.

Chitosan-clay nanocomposite was studied to remove Cd (II) and Cr (III) the obtained maximum sorption capacity was 72.31 mg g^{-1} on and 0.25 mg g^{-1} respectively. Bentonite-nZVI nanocomposite has also used an adsorbent for Cr (VI) removal the maximum uptake ability was found to be 296 mg g^{-1}. Humic acid-immobilized-amine modified polyacrylamide-bentonite (HA-Am-PAA-B) was also used as an adsorbent for Cu (II) removal by various researchers. From those results, the maximum removal efficiency was 106.2 mg g^{-1}. This capacity was obtained by changing the pH value from 6.2 to 5. The HA-AmPAA-bentonite nanocomposite was also used as an adsorbent for Zn (II) and Co (II) and the maximum removal capacity was 96.1 mg g^{-1} and 52.9 mg g^{-1} respectively [4].

The pH of a given solution can highly influence the adsorption process and capacity. It controls many important aspects such as the surface layer charge of the clay and the exchange capacity. Generally, the removal of heavy metals by the clay and clay-based nanocomposites initially increases with pH followed by a reduction until certain such a cut-off value of pH. The adsorption process is also temperature-dependent. Temperature can control the adsorption capacity of heavy metals onto clays and their nanocomposites [95].

2.7. Graphene Oxide

Graphene oxide (GO) is a carbon family material. These are single-layer graphene nano plastics connected by oxygen-containing functional groups. This material can be synthesized by a variety of methods, such as chemical oxidation or graphite exfoliation [96]. GO has many excellent properties, such as high specific surface area, high electrical conductivity, and thermal conductivity [97]. It also contains functional groups such as epoxy, hydroxyl, carbonyl, and carboxyl groups, these oxygen groups on the surface of GO ensure the

hydrophilicity and negative charge density of the surface, which is very useful for removing contaminants [98]. In the past, functionalized graphene was used to remove heavy metal ions [29] like lead and cadmium ions [38]. The adsorption affinity of GO for many metal ions is very high and varies with the type of heavy metal ions. The affinity of GO for Cu (II), Zn (II), Cd (II), and Pb (II) corresponds to Pb (II) Cu (II) ≫ Cd (II) Zn (II) [99]. This sequence is in good agreement with the electronegativity of the metal and the first stability constant of the corresponding metal hydroxide [100]. Figure 2.14 (a) and (b) show the structure of GO and its interaction with heavy metal cations, respectively.

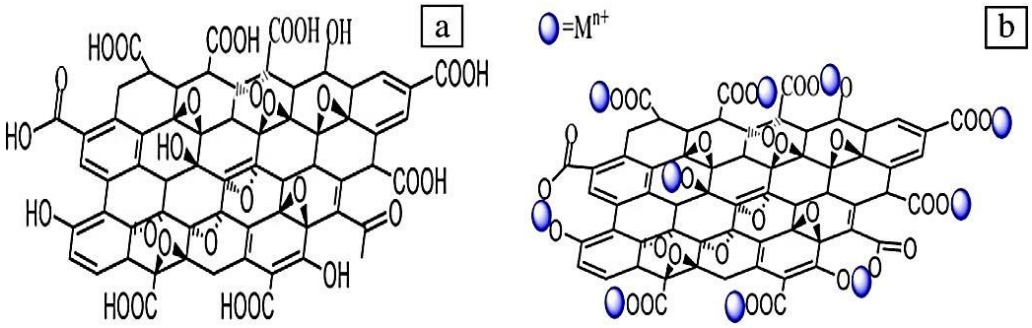

Figure 2.14. Structure of GO (a) and its interaction with heavy metal cations (b) [101].

The attraction of heavy metal ions to the negatively charged GO surface is stronger. In addition, the formation of complexes between heavy metal substances and surface oxygen-containing functional groups (such as -OH and -COOH) is also a possible adsorption method, and the morphology of heavy metal particles is determined by the stability constant GO is a suitable choice for modifying other absorbents (such as montmorillonite) [102].

The electrostatic attraction between the positively charged heavy metal ions and negatively charged GO sheets provides a driving force for the adsorption. Ion exchange reaction between heavy metal ions and the proton on –COOH or –OH oxygenous functional groups is one mechanism for the adsorption. The proton on –COOH or –OH was released to the solution in the adsorption process, leading to a lower equilibrium solution pH than the initial value [103, 104]. Surface complexation between heavy metal ions and surface oxygenous functional groups had been confirmed to play a dominant role in the adsorption of Pb(II) on GO [30]. The oxygenous functional groups located at the edges of GO sheets mainly participated in the complexation of Pb(II), and the Pb(II) bridged different GO sheets by simultaneously bonding

the hydroxyl or carboxyl groups at the edges [105]. The dispersibility of nano-sized GO makes it difficult to separate from water by using conventional separation methods (such as precipitation, filtration, and centrifugation). It has been proposed to add magnetic nanoparticles to GO and its compounds to easily separate solids from liquids under the influence of external magnetic fields [38, 101].

Even though Kaolinite clay is an efficient and available adsorbent for the elimination of heavy metal ions these adsorbent does not have magnetic properties. This leads to a limitation for reusability for many cycles of operation. To improve the recyclability of kaolinite, magnetic particles ($CoFe_2O_4$) can be added to the Kaolinite clay due to the easy separation of their composites by applying an external magnetic field. However, $CoFe_2O_4$ has agglomeration challenges, which can be minimized by synthesizing the magnetic spinel ferrites using a cellulose template and through the addition of graphene oxide (GO). To the best of our knowledge, there is no report on the synthesis of cellulose template $CoFe_2O_4$/Graphene oxide using *Ensete ventricosum* as a cellulose source, and composites of ternary $CoFe_2O_4$/Graphene oxide/Kaolinite for adsorption of lead ion is not done before this research. In addition, locally collected kaolinite clay was not used previously for any research. Generally, this research is done to contribute to the fulfillment of the above gaps i.e. reusability of kaolinite clay and agglomeration of $CoFe_2O_4$ particles for enhanced adsorption activity.

CHAPTER THREE

3. Materials, Chemicals, and Methods

3.1. Materials and Chemicals

For this work, analytical grade chemicals such as ferric nitrate nonahydrate ($Fe(NO_3)_3.9H_2O$), cobalt nitrate hydrate ($Co(NO_3)_2.6H_2O$, sodium hydroxide (NaOH), graphite powder, potassium permanganate ($KMnO_4$), sulfuric acid (H_2SO_4), phosphoric acid (H_3PO_4), hydrochloric acid (HCl), formic acid (CH_2O_2), acetic acid (CH_3 COOH), N, N-dimethylformamide (DMF), hydrogen peroxide (H_2O_2), distilled water, and ethanol were used. The clay was collected from Wollega, Ethiopia. In addition, the false banana by-product was collected from Adama City, Ethiopia.

3.2. Methods

3.2.1. Pretreatment of Clay

The collected clay (Figure 3.1a) was washed via distilled water (DH_2O) and dried in an oven at 90 °C overnight. After that, the dried clay powder was subjected to pass a 75 mesh sieve to obtain a fine powder (Figure 3.1b).

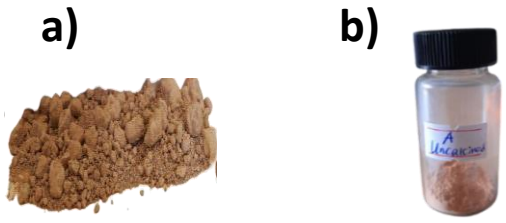

Figure 3.1. (a) collected clay and (b) pretreated clay.

3.2.2. Cellulose Extraction

The false banana byproduct was washed to remove dust, dried in an oven at 80 °C, cut, and then treated with extraction solvents in three stages [106, 107] as described below.

3.2.2.1. Alkaline Pretreatment (Stage I)

First, the false banana byproduct was boiled with 2% NaOH (1:40) w/v for 2 h to remove the remaining dust. Alkaline pretreatment was conducted in 3.0 L 5% NaOH solutions in a 1:10 (w/v) solid to liquid ratio of dry material on a hot plate at 90 °C for 1.5 h. Residues of the byproduct were filtered and washed continuously with hot distilled water.

3.2.2.2. Formic Acid, Acetic Acid, and Hydrogen Peroxide Treatment (Stage II)

The pulps were further treated with a mixture of 20% formic acid (FA)/20% acetic acid (AA)/7.5% H_2O_2 (2:1:2) solution on the hotplate at 90 °C for 1.5 h, at a byproduct to liquor ratio of 1:10. Finally, the delignified pulps were filtered to separate the cooking liquor (which contains lignin and hemicellulose) from cellulose and washed with hot water. Figure 3.2 shows the overall procedures for extracting cellulose from false bananas.

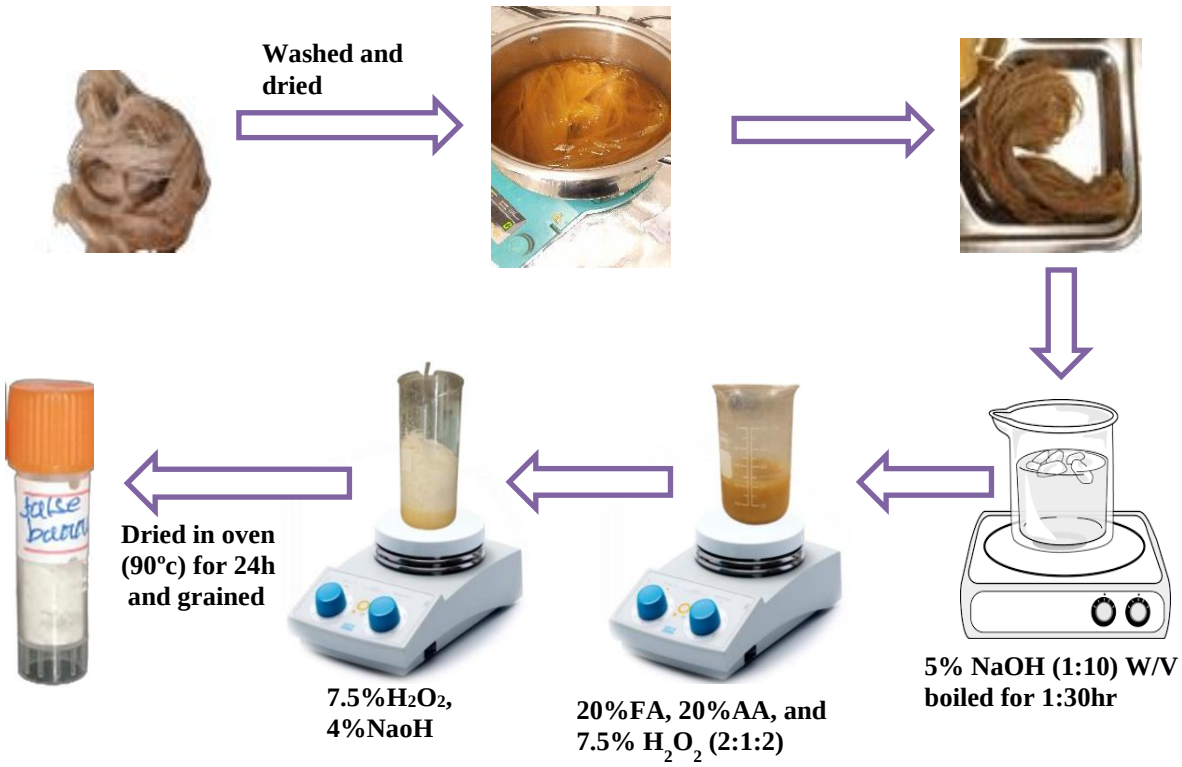

Figure 3.2. The diagram of procedures for extracting celluloses from false banana

3.2.2.3. Bleaching (Stage III)

Bleaching was done by treating the pulps with 7.5% H_2O_2 in alkaline media of 4% and 10% NaOH solutions at 1:10 fiber ratio separately, first at room temperature for 30 min, then on a water bath at 70 °C for 30 min. Finally, the pulps were washed repeatedly with hot distilled water to remove residual lignin and dried in an oven at 60 °C until a constant weight was achieved.

3.2.3. Synthesis of Graphene Oxide (GO)

Graphene oxide (GO) was synthesized from graphite powder via an improved method, as shown in Figure 3.3 [108]. The first stage involves using $KMnO_4$ as the oxidizing agent to oxidize graphite. For this purpose, 360 ml H_2SO_4 and 40 ml H_3PO_4 are introduced into an Erlenmeyer flask under constant and vigorous stirring. Then slowly about 9 g $KMnO_4$ and 3 g graphite (3:1) were added to the H_2SO_4/H_3PO_4 mixture by keeping the reaction mixture at 50 °C for 12 hours.

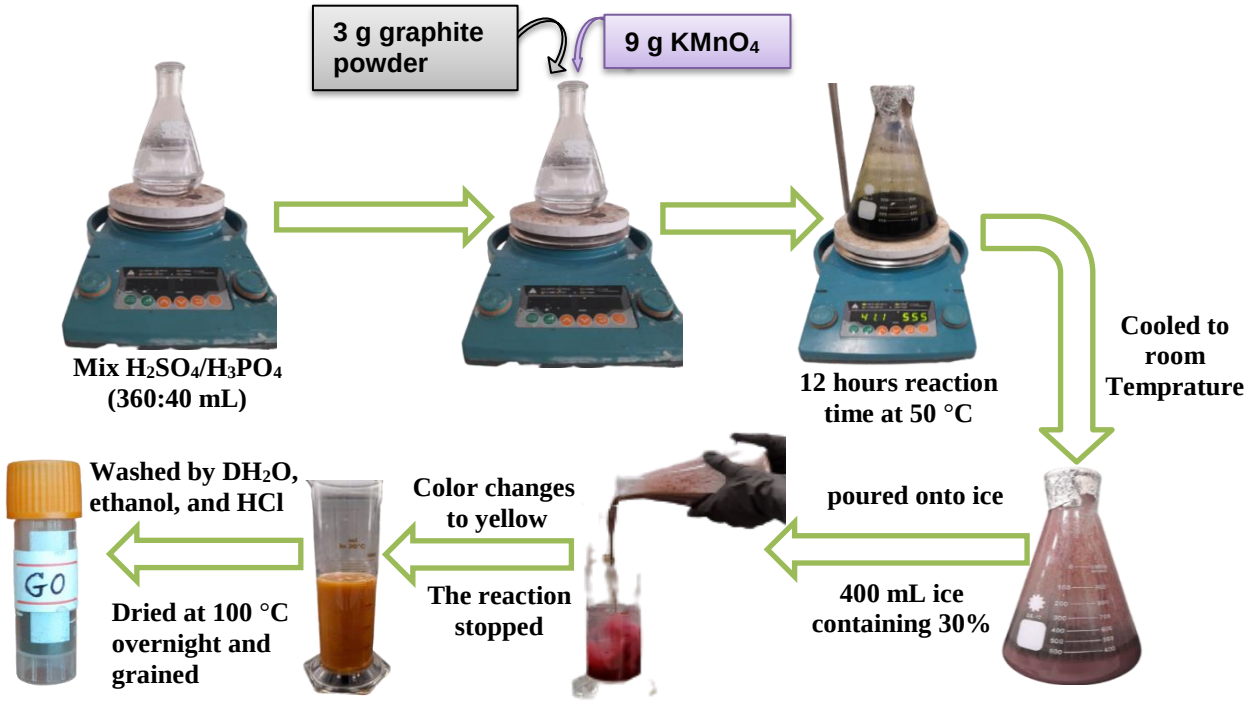

Figure 3.3. schematic procedure for the improved synthesis of graphene oxide (GO)

After the oxidation step, the resulting mixture was kept overnight in a beaker containing 400 g of ice flakes and 3 ml of H_2O_2 to stop the reaction of $KMnO_4$. The sample was centrifuged twice with deionized water (200 ml), HCl (200 ml), and ethanol (200 ml) to remove the

supernatant from graphene. Finally, the compacted cake was dried in an oven at 100 °C overnight.

3.2.4. Synthesis of Composites

Initially, binary composite (cellulose templated CF-GO) was synthesized by varying the weight percentage of GO, followed by ternary composite synthesis, which was formulated from kaolinite clay and the different weight ratios of $CoFe_2O_4$-0.3GO (CF-0.3GO).

3.2.4.1. Synthesis of Cellulose Templated CF-GO

CF-GO composite with different graphene content (20, 25, and 30 wt %) was synthesized by the hydrothermal method with some modification [109]. A measured amount of graphene oxide powder was added into 50 ml distilled water and 0.4 g cellulose into 25 ml distilled water in separate beakers and sonicated ultrasonically for 30 min to disperse the powders uniformly. The cellulose solution was poured into the GO solution followed by stirring for 30 min to form a homogenized solution. Then the appropriate amount of Fe $(NO_3)_3.9H_2O$ and Co $(NO_3)_2.6H_2O$ in a 2:1 ratio was added to the sonicated solution, followed by stirring for 60 min at room temperature. After that, 2M NaOH solution was dropped to the solution under constant stirring to adjust the pH around 10 then stirring for 10 min. The resulting mixture was transferred into a 100 mL Teflon-lined stainless autoclave and heated to 180 ºC for 12 h. The reaction mixture was allowed to cool to room temperature and the precipitate was centrifuged and washed with distilled water and ethanol several times. Finally, the solution was dried in an oven at 80 ºC for 12 h and then calcined at 400 ºC for 3 hours in a muffle furnace. For comparison, the same method was used to synthesize cellulose templated $CoFe_2O_4$ without adding GO.

3.2.4.2. Formulating Composites from Kaolinite Clay and $Cofe_2O_4$-GO Composite

After the synthesis of CF-GO, we formulated composite materials with kaolinite clay. First, the measured amount of kaolinite powder and different weight percent of CF-0.3GO (30, 45, 60, and 75 wt%) was dispersed by sonicating in 40 ml of N, N-Dimethylformamide in separate beakers for 30 min. Then uniform dispersion was obtained. After that CF-0.3GO solutions were transferred into kaolinite solution followed by sonication again for another 30

min. Then the solution was stirred for 3 h at room temperature to form a homogenized solution. Then, the obtained precipitate was centrifuged and washed with distilled water and ethanol several times. Finally, the prepared CF/GO/Kaolinite composite was dried at a temperature of 80 °C for 12 hrs.

3.3. Characterizations

The phase purity of adsorbents was examined using x-ray powder diffraction (XRD-700, Shimadzu, South Korea) using copper Kα radiation (λ_{CuKa} = 1.5418 Å), a scan speed of 4.0 deg/min, 40 kV, 30 mA, and a 2-θ scanning range from 4–80°. FTIR was used to identify functional groups from a wave number of 400–4000 cm^{-1} (FT/IR-4000 series, JASCO), and the thermal stability of the samples was investigated in a temperature range from 23 °C to 1000 °C using TGA-DTA (DTG-60H, Shimadzu, South Korea), and SEM (COXIEM-30, Shimadzu, South Korea). The adsorption capacity of the samples towards Pb (II) ion was examined using an AAS (ZEEnit 700P, Atomic Flame Mode, Analytik Jena).

3.4. Adsorption Performance Measurement

Lead standard solution, 1,000 mg L^{-1} Pb (II) in a diluted nitric acid standard for AAS (AVS TITRINORM) was used for adsorption study. Then a series of adsorption tests were carried out under typical equilibrium conditions. To select the best sample from the synthesized binary composites 4.5 mg adsorbents were added to a 50 mg L^{-1} concentration of 15 ml of Pb (II) solution in separate beakers. Then the samples were sonicated for 10 min, followed by stirring for 150 min. Effect of contact time was studied for the binary samples by adjusting the time from 30-90 min. In addition, adsorbent dosage for the binary samples was optimized by varying doses from 0.6-2.1 g L^{-1}. For the ternary composites, 22.5 mg adsorbent was used for 10 mg L^{-1} concentration of 15 mL Pb (II) solution. Effect of pH was also investigated by adjusting the pH values between the ranges 2-10 by adding 0.1 M NaOH and 0.1 M H_2SO_4. Kinetic studies were performed by adjusting the time from 30-120 min. Reusability of an adsorbent had been done by separating the adsorbents magnetically from the solution and washed several times by distilled water. Then allow to drying in an oven at 90°C for 3 h to reuse the adsorbent powder.

CHAPTER FOUR

4. Results and Discussions

4.1. Phase Purity Analysis

The XRD patterns of materials made of graphene oxide, $CoFe_2O_4$, and $CoFe_2O_4$-GO with different graphene content are shown in Figures 4.1. The diffraction pattern of graphene oxide shows a strong peak at 2θ = 11.3° (*d*-spacing of 7.76 Å) corresponds to the (001) plane which confirms the success in the GO synthesis [110]. It can be seen that the diffraction peaks of almost all $CoFe_2O_4$ with different graphene content can be traced back to spinel-like $CoFe_2O_4$ (JCPDS 022-1086).

The diffraction peaks at 2θ values of 18.3, 30.0, 35.4, 43.1, 53.5, 56.3, and 62.4, 71.1, 74.0, and 75.2 can be assigned to the crystal planes (111), (220), (311), (400), (422), (511), (440), (622), (533), and (620) of spinel $CoFe_2O_4$, respectively [111, 112]. Graphene (002) or GO (001) patterns are not observed in CF-GO. This can be explained by the reduction of GO to graphene during the hydrothermal and calcination process[109].

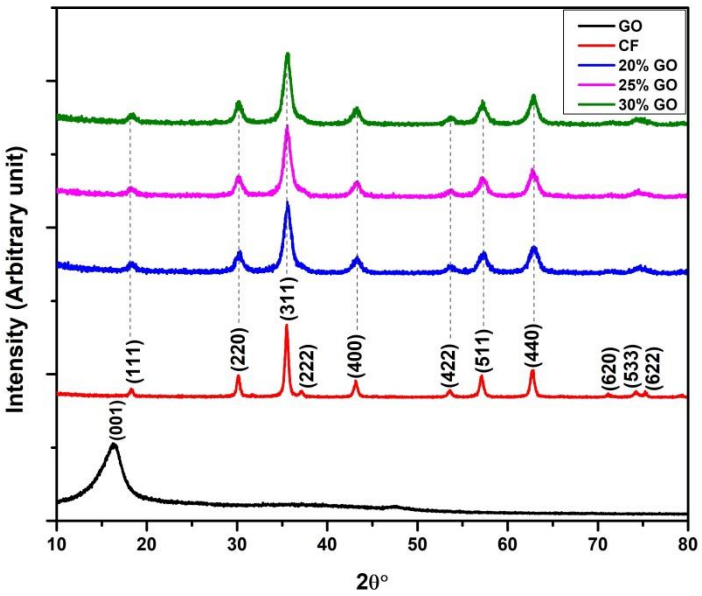

Figure 4.1. XRD pattern of, from bottom to top, graphene oxide (GO), CoFe2O4 (CF), CF-0.2GO, CF-0.25GO, and CF -0.3GO.

Moreover, the reduced GO layer may be peeled off and decorated the $CoFe_2O_4$ nanocrystals, resulting in the disappearance of the diffraction peak of graphene of the (002) crystallographic plane. The phase composition of the pretreated clay was determined by XRD. The 2θ diffraction pattern ranges from 10 to 80. The X-ray diffraction pattern of the pretreated clay is shown in Figure 4.2. JCPD files 058-2004 and 046-1045 indicate the existence of high-intensity diffraction peaks at 2θ of 12.39°, 19.85°, 24.96°, and 26.55°, the corresponding crystal orientation are (001), (020), (002), and (101), respectively [54, 113]. The JCPD document confirms that the main peaks of pretreated clay are kaolinite and quartz, which are usually found in kaolin as one of the main components.

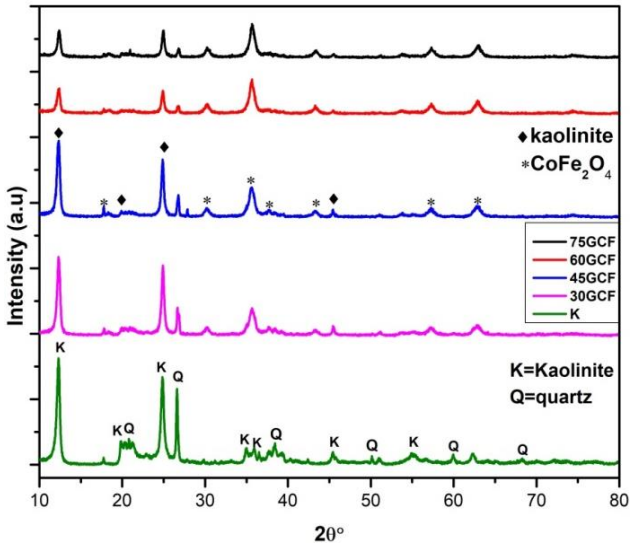

Figure 4.2. XRD pattern of, pure kaolinite and different composition of CF-0.3GO (GCF) in the kaolinite.

It is found that kaolinite ($Al_2Si_2O_5$ $(OH)_4$) has a very strong peak and a very good lifting peak; there is also a sharp quartz peak. Characteristic peaks in the X-ray diffraction pattern of kaolinite /($CoFe_2O_4$-0.3GO) samples with different weight fractions of $CoFe_2O_4$-0.3GO (30%, 45%, 60%, and 75%) is also shown in Figure 4.2. With an increase of GCF weight fraction, (001) peak intensity of kaolinite decreased, which indicates that a composite is effectively formed between kaolinite and ($CoFe_2O_4$-0.3GO). Like kaolinite powder, the ternary composites has sharp and significant peaks at 2θ of 12.39°, 19.85°, 24.96°, and 26.55° with the corresponding indices of (001), (020), (002), and (101), respectively. This indicates a high existence of kaolinite in these compounds (JCPDS. No. 058-2004) [114]. The diffraction

peaks of $CoFe_2O_4$ are also located at 2θ of 17.8, 30.5°, 35.5°, 43.2°, 57.1°, and 62.7° with corresponding(111), (220), (311), (400), (511), and (400) crystallographic planes, respectively, according to the crystallization level of JCPDS No. 022-1086.

4.2. Morphological Analysis

Figure 4.3 (a)-(e) shows the surface morphology of kaolinite (K), graphene oxide (GO), CF-0.3GO (without cellulose), CF-0.3GO (with cellulose) and 0.25K/0.75[(CF-0.30GO)], respectively. Figure 4.3a shows several layers of kaolin in which the kaolin particles are distributed with fewer aggregations. These results also showed some porous structure of the kaolinite lattice. As shown in Figure 4.3b layers of GO sheets were well exfoliated. The $CoFe_2O_4$/GO particles without cellulose template synthesis showed high agglomeration and larger particle size due to the magnetic property of $CoFe_2O_4$. In contrast, the $CoFe_2O_4$/GO composite with cellulose template synthesis showed a smaller particle size with porous morphology. This is happening because cellulose is a biopolymer with long chains and protects the formation of high agglomeration during synthesis as exhibited in Figure 4.3d. In addition, the porous structure is also exhibited in this morphology. Although the particles were homogenous they were aggregated at some point as seen in the SEM image. Unlike the kaolinite clay, Figure 4.3e shows the uniform distribution of smaller particles which may indicate the CF-0.3GO distributed evenly throughout the surface of kaolinite clay and modify the kaolinite structure.

+

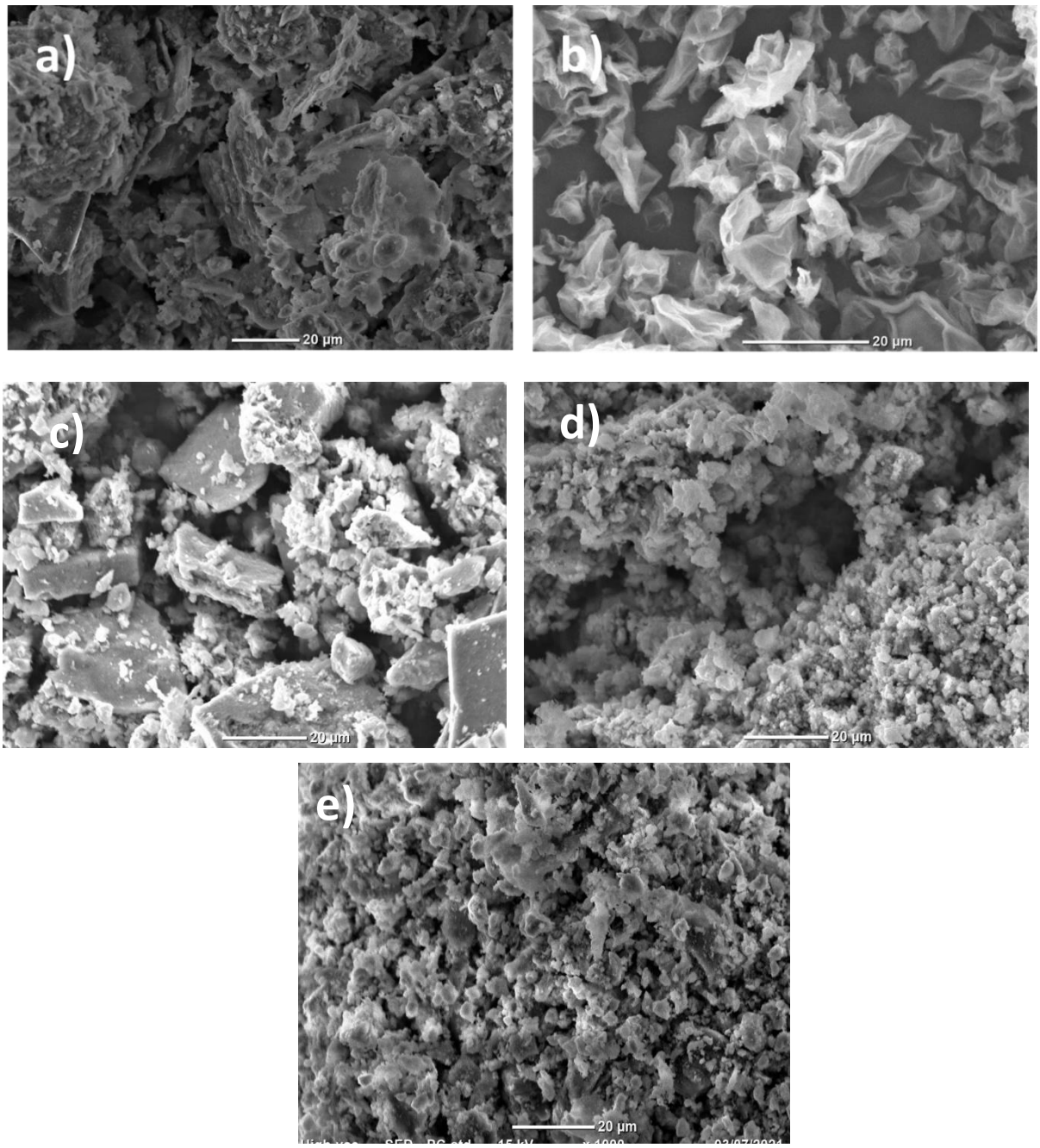

Figure 4.3. (a) The surface morphology of (a) kaolinite (K), (b) graphene oxide (GO), (c) CF-GO (without cellulosee), (d) CF-0.3GO (with cellulose) and (e) K/CF-GO.

4.3. FTIR Analysis

FTIR spectra of the GO, CF-GO, K, and K/(CF-GO)were examined to determine the presence of functional groups. For GO (Figure 4.4a), the broad peak at 3416 cm^{-1} corresponds to O□H

stretching vibration. In addition, the five peaks at 1726, 1584, 1403, 1221, 1048 cm^{-1} belong to C=O stretching, aromatic C□C, C□O carboxyl, epoxy C□O and alkoxy [115, 116]. For CF-GO, the stretching vibration O□H indicates that the peak is narrower than that of GO, and the peaks of oxygenates are quite attenuated or completely attenuated, indicating that the GO content in the CF-GO compound may be reduced [109], and the adsorption peak near 1622 cm^{-1} can be traced back to the stretching vibration of the non-oxidized carbon.

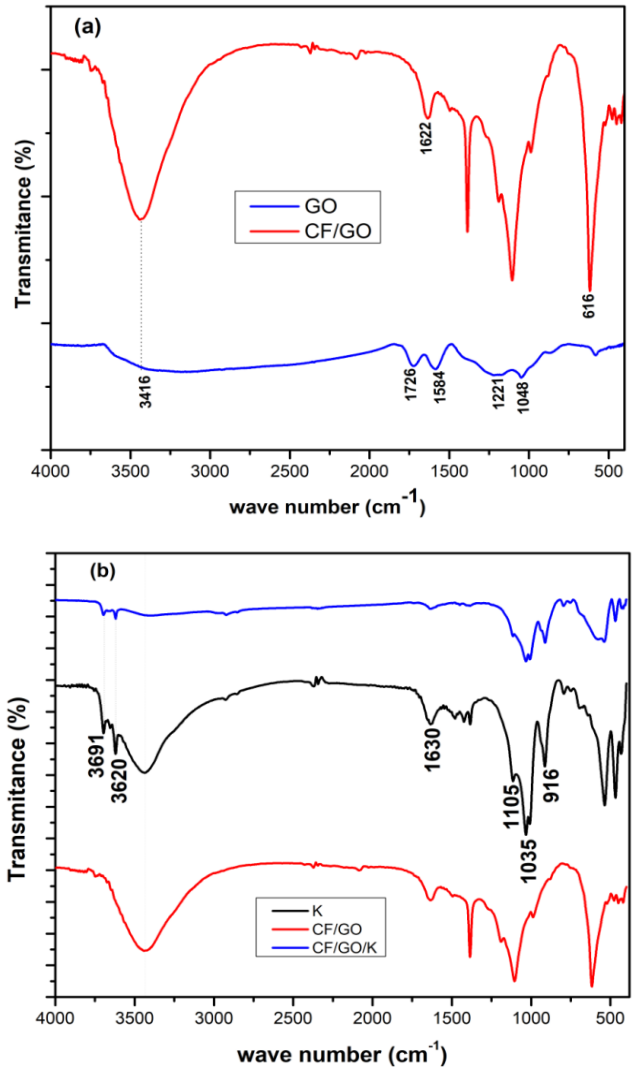

Figure 4.4. FTIR spectra of the (a) GO, CF/GO (CF-0.3GO), and (b) , K (kaolinite), CF/GO/K 0.25K/0.75[(CF-0.30GO)], and CF/GO samples.

The result of 616 cm^{-1} shows that CF/GO corresponds to the valence vibrational bond of Co□O and Fe□O (metal-oxygen bond). The FTIR spectrum of the kaolinite was shown in

Figure 4.4b. It shows absorption bands at 3691 and 3620 cm^{-1}, which are due to the OH stretching vibration, and the absorption at 1630 cm^{-1}, 1035 cm^{-1}, 1105 $cm^{-1,}$ and 916 cm^{-1} have an H-O-H interlayer, a tetrahedral sheet of Si-O-Si group, stretching vibration Si-O and Al-OH, respectively [117]. The peaks at 750 and 467 cm^{-1} correspond to quartz, while the bands at 430 cm^{-1} in kaolinite correspond to the tensile modes of Si-O, Al-O, and Si-O-Si bonds. This information provides a functional interface group involved in the adsorption process of kaolinite. The CF/GO/K peak at 1622 cm^{-1} is significantly reduced, indicating that there is a strong interfacial interaction between GO, CF, and K, which improves the mechanical strength of the composite [118]. After the kaolinite was corrected with GO and $CoFe_2O_4$, the peak area and intensity of the obtained composite material changed significantly, which may depend on the interaction between the functional groups in GO and the kaolinite structure [119].

4.4. Thermal Property Analysis

Figure 4.5 (a)-(c) exhibit thermal analysis of kaolinite, $CoFe_2O_{4,}$ and K/CF-GO composite sample from room temperature up to 800 °C. All samples show different weight loss stages, which can be seen in the TGA and corresponding DTA curves. The first stage of weight loss, for kaolinite, $CoFe_2O_{4,}$ and K/(CF-GO) is about 3.29 %, 2.55 %, 1.88 %, which corresponds to the evaporation of water molecules from the surface into a crystalline structure [120]. The second weight loss is related to the dehydration (dehydroxylation) of coordinated water molecules and the decomposition of clay. This is because of the decomposition of organic components present in the material in the sample, for the Kaolinite and K/(CF-GO). The second weight loss of CF may be due to the decarburization of the cobalt ferrite particles [121]. The overall weight loss of CF was about 4.1 % and the thermal stability of CF can reach up to 800°C**.**

At the second stage of weight loss, the onset temperature (T_{onset}) is about 426 °C, 150 °C, and 400 °C, respectively, for K, CF, K/CF-GO samples. In the same stage of weight loss, the corresponding finishing temperature (T_{finish}) is about 616 °C, 500 °C, and 700 °C, for K, CF, and K/CF-GO samples, respectively. The overall weight loss of Kaolinite was about 13.67 %, while that of the K/CF-GO was about 6,31 %. These suggest that the thermal stability of K/CF-GO is enhanced with the incorporation of stable CF particles into the kaolinite.

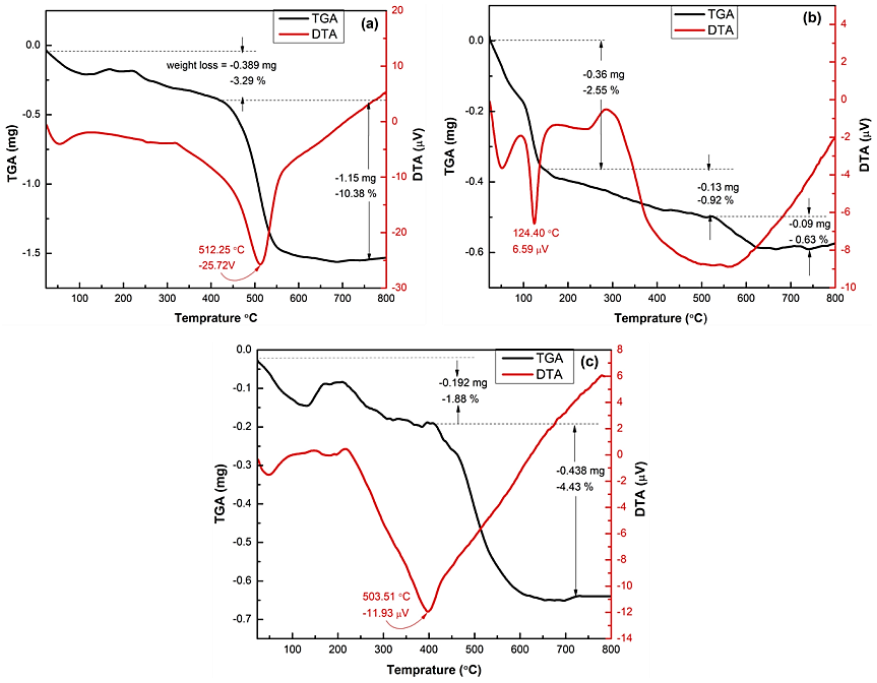

Figure 4.5. TGA-DTA analysis of (a) kaolinite (K), (b) $CoFe_2O4$ (CF), and (c) K/CF-GO 0.25K/0.75[(CF-0.30GO)].

4.5. Magnetic Property of $CoFe_2O_4$-Graphene/Kaolinite Adsorbents

The magnetic properties of $CoFe_2O_4$ enhance the separation for the prepared composites. We studied the magnetic separation properties of the $CoFe_2O_4$-Graphene/Kaolinite adsorbents. As shown in Figure 4.6, the catalyst with homogeneous dispersion was strongly responsive to an external magnetic field, which can be easily separated from the reaction mixture in less than 1 minute using a permanent magnet.

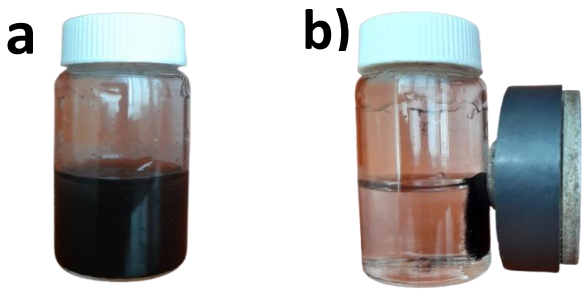

Figure 4.6. Images of 0.75[(CF-0.3GO)/0.25K suspension with (a) and without (b) a magnetic field.

4.6. Adsorption Performance Analysis

To determine the adsorption behavior of the composite, a series adsorption test was carried out with compositions (1–x)CF/(x)GO (x=0.20, 0.25, 0.30, weight percentage of GO). The removal efficiency/adsorption (%) and adsorption capacity of the materials can be calculated according to equations (1) and (2) as follows [70]:

$$\text{Adsorption}(\%) = \frac{C_i - C_f}{C_i} \times 100 \qquad (1)$$

$$q_e(\%) = \frac{V(C_i - C_e)}{M} \qquad (2)$$

where C_i and C_f are the initial and final metal ion concentration; q_e and C_e are equilibrium adsorption capacity and concentration of the metal ions at equilibrium; V is the volume of metal ion solution (L) and M is the mass of adsorbent in grams.

The adsorption capacity of (1–*x*)CF/(*x*)GO with *x*=0.20, 0.25, and 0.30 weight ratios of GO is shown in Figure 4.7. Among the composites, the sample with x = 0.3, i.e., CF-0.3GO had shown the highest adsorption capacity of about 23.6 mg g^{-1}. As a result, this sample was selected for further studies and named GCF.

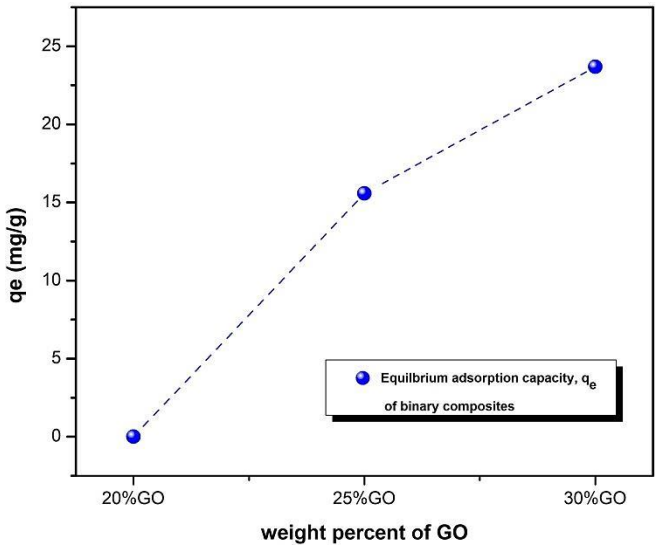

Figure 4.7. The equilibrium adsorption capacity of CF-GO composites with different GO loading initial concentrations of 50 mg L^{-1}, at a temperature of 25 ºC.

As shown in Figure 4.7, the adsorption capacity of Pb (II) using CF-GO increased as the amount of GO increased. Moreover, graphene oxide has a large surface area and contains many functional oxygen groups, such as hydroxyl and carboxyl groups [67, 122]. Therefore, with the increase of GO, the increase in the adsorption capacity of Pb (II) can be explained by the increase in surface area and surface-active sites of the adsorbent [123, 124]. This result indicates that the addition of graphene oxide improves the adsorption performance of CoF_2O_4 on Pb (II).

4.6.1. Effect of Contact Time and Adsorbent Dosage on GCF

The contact time required to effectively remove contaminants from the adsorbent is important to determine the optimum time to remove heavy metal ions. The effect of contact time on the decrease of Pb (II) content in GCF is shown in Figure 4.8a. Pb adsorption is carried out in GCF, Ci = 10 mg L^{-1} and adsorbent dose = 300 mg L^{-1} to optimize the contact time between ions and adsorbent at room temperature. Initially, the adsorption rate of Pb (II) increases rapidly with time and then reaches equilibrium.

The adsorption occurs quickly, due to the presence of active and vacant sites on the surface of the adsorber in the initial stage [119]. Figure 4.8a clearly shows that the optimal Pb removal time is 90 min. At this time, the adsorption rate is equal to the desorption rate, and as the duration increases; the active site is inaccessible, which leads to a decrease in the driving force and a decrease in the adsorption rate [38]. However, a further increase in contact time indicates a decrease in the percentage of Pb. This temporary effect may be related to the saturation of the adsorbent surface with metal ions, followed by the adsorption and desorption process [54]. Therefore, 90 min is considered the best time to optimize the adsorbent dosage of GCF.

In the adsorption procedure, the adsorbent dose is just one of the essential variables which can establish the adsorption efficiency and capacity. The effect of the GCF adsorbent dosage on the removal of Pb ions was studied by increasing the dosage from 0.6-2.1 g L^{-1} (Figure 4.8b).

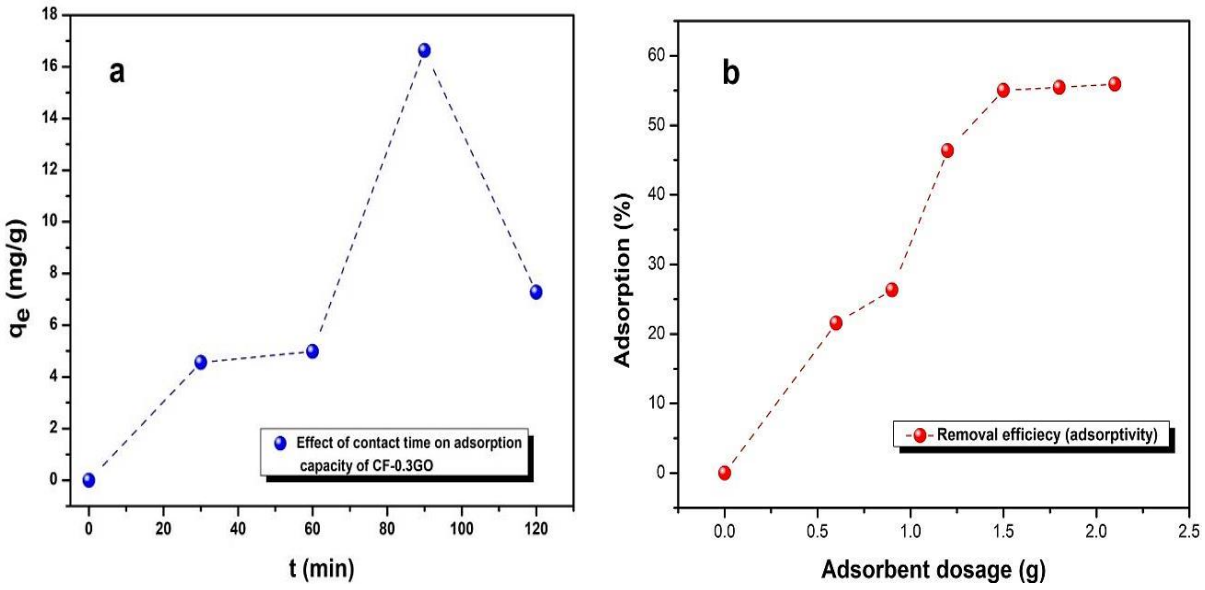

Figure 4.8. Effect of (a) contact time and (b) adsorbent dosage on the percentage of lead ion on to GCF, initial concentration of 10 mg L^{-1}, T=25ºC.

The elimination effectiveness of Pb ions was raised with a rise of adsorbent dose, which can be associated with the existence of a lot of active sites on the surface of adsorbent for adsorption [125]. As all the active sites might not be readily available for adsorption, it will lead to saturation.

The saturation factor for Pb(II) ions was located at 1.5 g L^{-1} for GCF with 55% mg g^{-1} removal effectiveness. As a result, 1.5 g L^{-1} adsorbent was taken as the optimal adsorbent dosage values for more detailed examinations. After optimizing the contact time and the dose of the binary compound (GCF), the ternary composites i.e (y)[(CF-0.30GO)]/(1-y)K, where y = 0.3, 0.45, 0.60, and 0.75, were synthesized. Then the adsorption capacity was also evaluated. Figure 4.9 shows the adsorption capacity for the synthesized ternary composites.

A sample with the composition of 0.25K/0.75[(CF-0.30GO)] showed the highest adsorption capacity among other composite materials, about 4.2 mg g^{-1}. Then this sample is used for other studies, such as changes in pH, contact time, and adsorption kinetics.

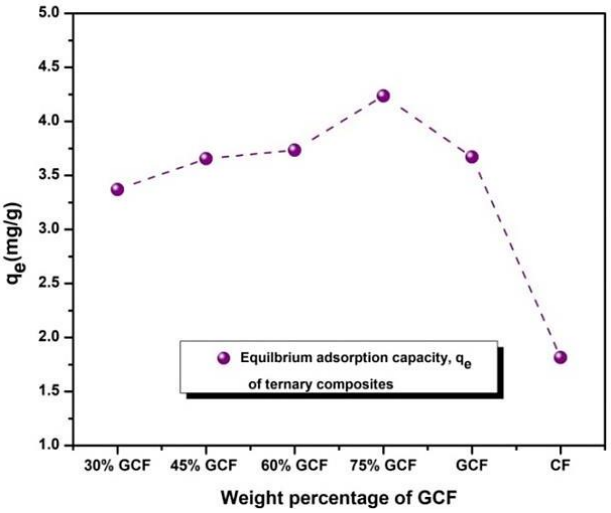

Figure 4.9. Adsorption capacity (qe) of $CoFe_2O_4$ (CF), CF-0.3-GO (GCF), and K/GCF composites with different GCF loading on kaolinite, initial concentration of 10 mg L^{-1}, T=25ºC.

4.6.2. Effect of pH and Contact Time for the Ternary Composite

Taking into account the influence of pH value, the adsorption performance of 0.25K/0.75[(CF-0.30GO)] was analyzed, because this has a direct effect on the adsorption performance. The initial concentration of both metal ions at 25°C is 10 mg L^{-1}. The pH range of Pb ions with the same metal ion concentration is 2 to 10. Figure 4.10a shows that the adsorption increases with the increase of pH under acidic conditions (2-4) significantly, and then reaches a peak at pH 4

and then all points are flatted. At pH 4, the adsorption capacity and removal efficiency become 6.6 mg g^{-1} and 99%, respectively.

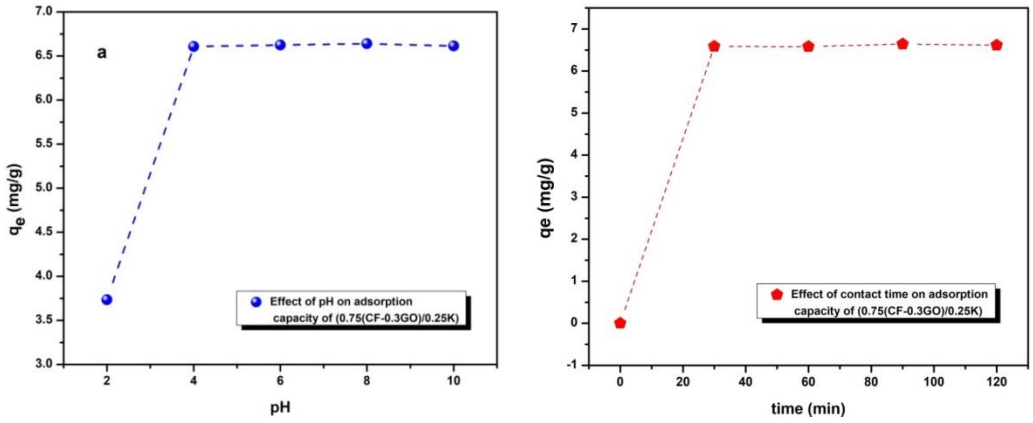

Figure 4.10. Effect of (a) pH (b) contact time on percentage of lead adsorption onto 0.25K/0.75[(CF-0.30GO)] composite material, initial conc. 10 mg/L,T = 25 °C

At low pH (pH = 2), the removal ability of the Pb ion was low, which may be due to the high concentration of H^+ ion in the medium, so the ion occupies the active sites [126]. The initial pH value increases, the amount of H^+ in the medium decreases, and the competition between H^+ and metal ions on the adsorber surface might be reduced, which significantly improves the efficiency of the adsorption method [127].

The percentage of Pb (II) adsorbed onto the present composite was also examined as a function of contact time (Figure 4.10b). First, the adsorption rate of Pb (II) increases rapidly with time, and the adsorption capacity becomes higher after 30 minutes. Then there is an almost small increase in adsorption rates. Compared with the adsorption from 30 minutes to 120 minutes, the adsorption capacity after 90 minutes was 6.64 mg g^{-1}, as a result, the 90 min time was chosen as the equilibrium time for the kinetic study.

4.6.3. Adsorption Kinetics

To study the mechanism of controlling adsorption, a kinetic model suitable for data analysis, mass transfer, and chemical reactions are needed. In this study, the adsorption data corresponds to two kinetic models: Lagergren pseudo-first-order and pseudo-second-order. The calculated data in Table 4.1 was used to study the kinetic models. The first-order kinetic

model is suitable for solid-liquid systems, and the system equation can be expressed as below [128-130].

Table 4.1. Parameters for plotting adsorption kinetics for the sample of 0.25K/0.75[(CF-0.30GO)]

Time (min)	q_e (mg g^{-1})	q_t (mg g^{-1})	q_e-q_t	Log(q_e-q_t)	t/q_t
30	6.64	6.586	0.054	-1.267606	4.554
60	6.64	6.58	0.06	-1.221848	9.117
90	6.64	6.64	0.0	-	13.533
120	6.64	6.61	0.03	-1.522878	18.147

For the Pseudo-first-order, the corresponding equation can be written as:

$$log(q_e - q_t) = log - \frac{k_1}{2.303} t \qquad (3)$$

where, q_e and q_t are the adsorption capacity (mg g^{-1}) at equilibrium and time t, respectively, and k_1 is the rate constant of the pseudo-first-order kinetic model. The k_1 and q_e values can be calculated from the slope and intercept of the plot of log (q_e-q_t) against *t*.

For the Pseudo-second-order, the corresponding equation can be written as:

$$\frac{t}{q_t} = \frac{1}{k_2 q_e^2} + \frac{1}{q_e} t \qquad (4)$$

Where q_e and q_t are the sorption capability (mg g^{-1}) at equilibrium and time *t*, respectively, and k_2 is that the rate constant of the pseudo-second-order kinetic model. The k_2 and qe values may be calculated from the intercept and slope of the plot of t/q_t against *t*. Figures 4.11 a and b show the linear diagrams of the pseudo-first-order and pseudo-second-order kinetic models of Pb (II) adsorption on 0.25K/0.75[(CF-0.30GO)], respectively.

The values of the correlation coefficient (R^2) obtained from the linear fitting curve of each model are provided and Table 4.2 summarizes the fitting parameters. For all adsorbents, the R^2 values obtained from the pseudo-first-order model are very low (R^2 = 0.99488).In contrast, the pseudo-second-order model is more consistent with the experimental data with R^2 = 0.9999.

Furthermore, the calculated equilibrium adsorption capacity ($q_{e,(cal)}$) is very consistent with the experimental equilibrium adsorption capacity ($q_{e,(exp)}$).

Based on these results, the pseudo-second-order kinetic model can better describe the adsorption of Pb (II) in 0.25K/0.75[(CF-0.30GO)]. The pseudo-second-order kinetic model is based on the assumption that the rate-limiting step is controlled by chemical adsorption [131]. This indicates that the adsorption of Pb(II) on 0.25K/0.75[(CF-0.30GO)] composite is controlled by chemical adsorption.

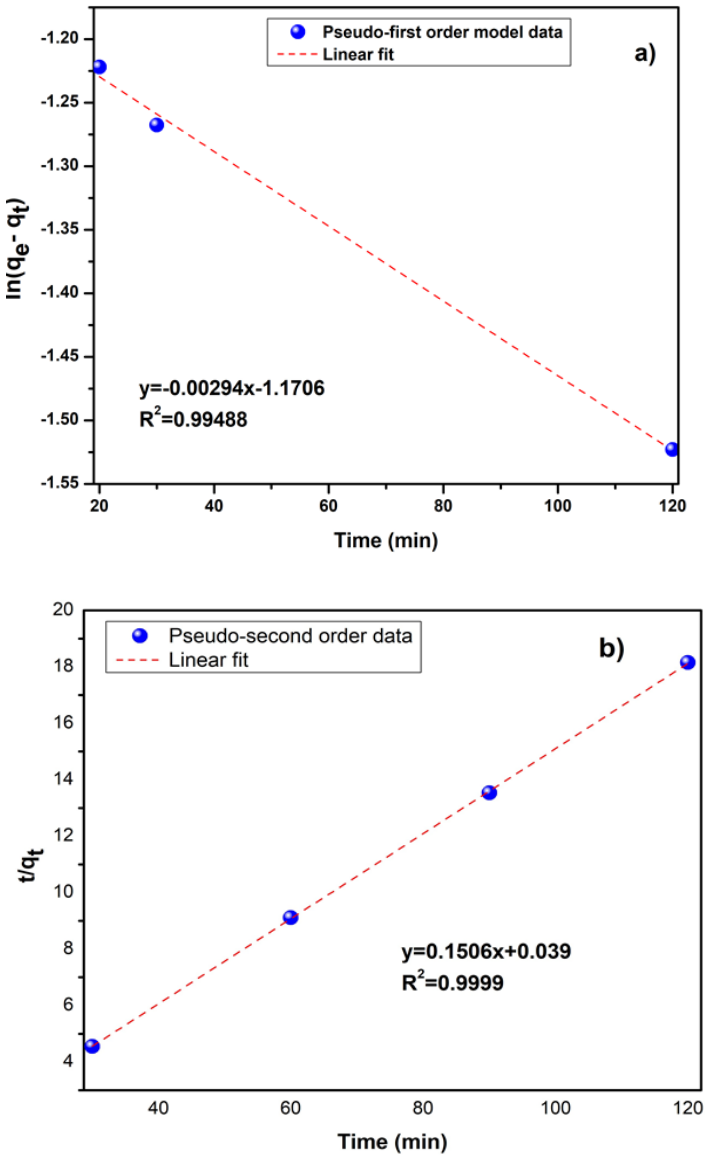

Figure 4.11. Pseudo-first-order kinetic models for 0.25K/0.75[(CF-0.30GO)] composite material.

Table 4.2. Calculated parameters from Pseudo-first and Pseudo-second-order kinetic models for the sample of 0.25K/0.75[(CF-0.30GO)] composite material.

Model	Parameters	Values	R^2
Pseudo-first-order	*qe,exper.* (mg g^{-1})	0.06751	0.99488
	qe,calc. (mg g^{-1})	6.6405	
	K_1 (min^{-1})	-0.0000564	
Pseudo-second-order	*qe,exper.* (mg g^{-1})	6.6401	0.9999
	qe,calc. (mg g^{-1})	6.6405	
	K_2 (min^{-1})	0.5815	

4.6.4. Reusability of the Adsorbent

The 0.25K/0.75[(CF-0.30GO)] adsorbent was tested for up to three adsorption-desorption cycles for the reuse of Pb (II) aqueous solution (Figure 4.12). The test was done at the optimized pH value (at pH of 4) and reaction time (90 min) at room temperature. The results show that as the adsorption-desorption stage increases, the adsorption percentage of Pb (II) decreases. This decrease in efficiency may be related to the damage or change of the active center of the adsorber [132]. The removal efficiency of the lead ion using the present adsorbent was 99.5, 99.4, and 96.2 % in the first, second, and third cycles, respectively. In addition, it should be noted that at the third cycle of the adsorption process, the reduction in the amount of Pb (II) adsorption using the adsorber is less than 4%. The results show that the obtained adsorbent can be used for up to three cycles to remove lead ions from an aqueous solution without significantly reducing the adsorption capacity.

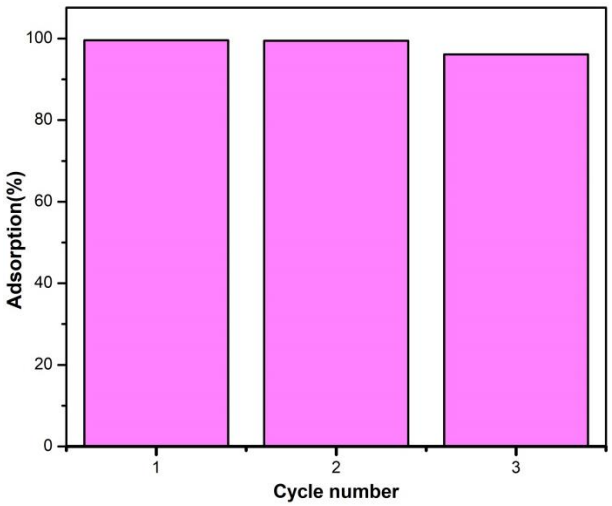

Figure 4.12. Effect of recycling 0.25K/0.75[(CF-0.30GO)]on the adsorption efficiency.

5. Conclusion and Recommendation

5.1. Conclusion

In this study, Graphene oxide, $CoFe_2O_4$, $CoFe_2O_4$-GO (CF-GO), and K/(CF-GO) were successfully synthesized by improved, hydrothermal, and solution methods, respectively. Among the binary composites, CF-0.3GO showed a better adsorption capacity of about 23.6 mg g^{-1} from the binary composite samples at the initial Pb concentration of 50 mg l^{-1}. In addition, the sample with a composition of 0.25K/0.75[(CF-0.30GO)] showed the best adsorption capacity of about 4.2 mg g^{-1} at the initial Pb concentration of 10 mg l^{-1} from the ternary composites and was selected for further studies. The materials were characterized using XRD, SEM, FTIR), and TGA-DTA. The XRD results showed that the pretreated clay was contained a high content of kaolinite clay with little quartz amount. The XRD pattern of the synthesized $CoFe_2O_4$ and GO confirmed the formation of pure $CoFe_2O_4$ particles and graphene oxide. The effective formation of the ternary composite was also confirmed by the XRD results. The FTIR data of (CF-GO)/K confirmed the presence of various oxygen-containing functional groups which enhance the adsorption capacity by the reactions of Pb (II) with active surface groups. TGA-DTA data revealed that the thermal stability of kaolinite enhanced with the incorporation of $CoFe_2O_4$ and GO through the structure. The effect of pH (2-10) and contact time (30-90min) were also studied for 0.25K/0.75[(CF-0.30GO)] composite. At pH of 4, the adsorption capacity and removal efficiency was 6.62 mg g^{-1} and 99 %, respectively, and becomes constant. The adsorption kinetics best fitted with Pseudo-second-order adsorption which indicates. Finally, the reusability of the present composite was studied after separating the catalyst magnetically for up to 3 cycles with a small reduction in removal efficiency. Therefore, the experimental results of this study specify that the present composite could be a potential candidate for the removal of Pb (II).

5.2. Recommendation

In this study, we investigated the adsorption capacity of K/(CF-GO) ternary composites towards lead ion (Pb (II)) removal from an aqueous solution. The results show that this composite has a good adsorption capacity to Pb (II). However, there are also other toxic to heavy metals such as mercury, arsenide, cobalt and so. We further recommend the investigation of the adsorption capacity of these ternary composites towards other toxic heavy metals. The adsorption performance of the synthesized materials is highly affected by the surface area and pore volume of the adsorbent. Therefore, we recommended the determination of specific surface area and porosity using Brunner-Emmet-Teller (BET).

References

1. Asadi, R., et al., *Effective removal of Zn (II) ions from aqueous solution by the magnetic $MnFe_2O_4$ and $CoFe_2O_4$ spinel ferrite nanoparticles with focuses on synthesis, characterization, adsorption, and desorption.* Advanced Powder Technology, 2020. 31(4): p. 1480-1489.
2. Fiyadh, S.S., et al., *Review on heavy metal adsorption processes by carbon nanotubes.* Journal of Cleaner Production, 2019. 230: p. 783-793.
3. Obayomi, K.S. and M. Auta, *Development of microporous activated Aloji clay for adsorption of lead (II) ions from aqueous solution.* Heliyon, 2019. 5(11): p. e02799.
4. Yadav, V.B., R. Gadi, and S. Kalra, *Clay based nanocomposites for removal of heavy metals from water: A review.* J Environ Manage, 2019. 232: p. 803-817.
5. Es-sahbany, H., et al., *Removal of heavy metals (Nickel) contained in wastewater-models by the adsorption technique on natural clay.* Materials Today: Proceedings, 2019. 13: p. 866-875.
6. Obasi, P.N. and B.B. Akudinobi, *Potential health risk and levels of heavy metals in water resources of lead–zinc mining communities of Abakaliki, southeast Nigeria.* Applied Water Science, 2020. 10(7): p. 184.
7. Monear, N.C. and B. Xhabija, *The effect of lead during the Flint water crisis on mouse embryonic stem cells self-renewal and differentiation markers.* Toxicology in Vitro, 2020. 63: p. 104719.
8. Triantafyllidou, S. and Y. Lambrinidou, *Lead (Pb) exposure through drinking water: Lessons to be learned from recent U.S. experience.* Global Nest Journal, 2009. 11.
9. Mnasri-Ghnimi, S. and N. Frini-Srasra, *Removal of heavy metals from aqueous solutions by adsorption using single and mixed pillared clays.* Applied Clay Science, 2019. 179: p. 105151.
10. Yadav, D.K. and S. Srivastava, *Carbon nanotubes as adsorbent to remove heavy metal ion (Mn^{+7}) in wastewater treatment.* Materials Today: Proceedings, 2017. 4(2, Part A): p. 4089-4094.

11. Hayati, B., et al., *Heavy metal adsorption using PAMAM/CNT nanocomposite from aqueous solution in batch and continuous fixed bed systems.* Chemical Engineering Journal, 2018. 346: p. 258-270.
12. Verma, B. and C. Balomajumder, *Surface modification of one-dimensional Carbon Nanotubes: A review for the management of heavy metals in wastewater.* Environmental Technology & Innovation, 2020. 17: p. 100596.
13. Deliyanni, E., et al., *Activated carbons for the removal of heavy metal ions: A systematic review of recent literature focused on lead and arsenic ions.* Open Chemistry, 2015. 13.
14. Kobya, M., et al., *Adsorption of heavy metal ions from aqueous solutions by activated carbon prepared from apricot stone.* Bioresource Technology, 2005. 96(13): p. 1518-1521.
15. Nejadshafiee, V. and M.R. Islami, *Adsorption capacity of heavy metal ions using sultone-modified magnetic activated carbon as a bio-adsorbent.* Materials Science and Engineering: C, 2019. 101: p. 42-52.
16. Lo, S.-F., et al., *Adsorption capacity and removal efficiency of heavy metal ions by Moso and Ma bamboo activated carbons.* Chemical Engineering Research and Design, 2012. 90(9): p. 1397-1406.
17. Lee, L.Z., M.A.A. Zaini, and S.H. Tang, *Porous Nanomaterials for Heavy Metal Removal*, in *Handbook of Ecomaterials*, L.M.T. Martínez, O.V. Kharissova, and B.I. Kharisov, Editors. 2019, Springer International Publishing: Cham. p. 469-494.
18. Yao, L., et al., *Green synthesis of mesoporous $ZnFe_2O_4$/C composite microspheres as superior anode materials for lithium-ion batteries.* Journal of Power Sources, 2014. 258: p. 305-313.
19. Boix, G., et al., *MOF-Beads Containing Inorganic Nanoparticles for the Simultaneous Removal of Multiple Heavy Metals from Water.* ACS Applied Materials & Interfaces, 2020. 12(9): p. 10554-10562.
20. Ray, P.Z. and H.J. Shipley, *Inorganic nano-adsorbents for the removal of heavy metals and arsenic: a review.* RSC Advances, 2015. 5(38): p. 29885-29907.

21. Giraldo, L., A. Erto, and J.C. Moreno-Piraján, *Magnetite nanoparticles for removal of heavy metals from aqueous solutions: synthesis and characterization.* Adsorption, 2013. 19(2): p. 465-474.
22. Lee, G.F., *Role of hydrous metal oxides in the transport of heavy metals in the environment*, in *Heavy metals in the aquatic environment*. 1975, Pergamon Oxford. p. 137-147.
23. Ghiloufi, I., et al., *Ga-doped ZnO for adsorption of heavy metals from aqueous solution.* Materials Science in Semiconductor Processing, 2016. 42: p. 102-106.
24. Kikuchi, Y., et al., *Effect of ZnO loading to activated carbon on Pb (II) adsorption from aqueous solution.* Carbon, 2006. 44(2): p. 195-202.
25. Chen, Q., et al., *Adsorption of cadmium (II) on humic acid coated titanium dioxide.* Journal of colloid and interface science, 2012. 367(1): p. 241-248.
26. Yadav, V.B., R. Gadi, and S. Kalra, *Clay based nanocomposites for removal of heavy metals from water: a review*. Journal of environmental management, 2019. 232: p. 803-817.
27. Das, S., et al., *Clay-based nanocomposites as recyclable adsorbent toward Hg (II) capture: experimental and theoretical understanding.* ACS omega, 2018. 3(6): p. 6283-6292.
28. Darder, M., M. Colilla, and E. Ruiz-Hitzky, *Chitosan–clay nanocomposites: application as electrochemical sensors.* Applied Clay Science, 2005. 28(1-4): p. 199-208.
29. Yari, M., et al., *Kinetics of the adsorption of Pb (II) ions from aqueous solutions by graphene oxide and thiol functionalized graphene oxide.* Journal of Molecular Liquids, 2015. 209: p. 50-57.
30. Zhao, G., et al., *Removal of Pb (II) ions from aqueous solutions on few-layered graphene oxide nanosheets.* Dalton transactions, 2011. 40(41): p. 10945-10952.
31. Tan, P., et al., *Adsorption of Cu^{2+}, Cd^{2+} and Ni^{2+} from aqueous single metal solutions on graphene oxide membranes.* Journal of hazardous materials, 2015. 297: p. 251-260.
32. *A review on the application of clay minerals as heavy metal adsorbents for remediation purposes.* Environmental Technology & Innovation, 2020.

33. Bhattacharyya, K. and S. Gupta, *Removal of Cu(II) by natural and acid-activated clays: An insight of adsorption isotherm, kinetic and thermodynamics.* Desalination, 2011. 272: p. 66-75.
34. Wu, L., et al., *Organo-bentonite-Fe_3O_4 poly(sodium acrylate) magnetic superabsorbent nanocomposite: Synthesis, characterization, and Thorium(IV) adsorption.* Applied Clay Science, 2013. 83-84: p. 405-414.
35. Yan, L., et al., *Facile solvothermal synthesis of Fe_3O_4/bentonite for efficient removal of heavy metals from aqueous solution.* Powder Technology, 2016. 301: p. 632-640.
36. Liu, X.-M., S.-Y. Fu, and L.-P. Zhu, *High-yield synthesis and characterization of monodisperse sub-microsized $CoFe_2O_4$ octahedra.* Journal of Solid State Chemistry, 2007. 180(2): p. 461-466.
37. Mathew, D.S. and R.-S. Juang, *An overview of the structure and magnetism of spinel ferrite nanoparticles and their synthesis in microemulsions.* Chemical engineering journal, 2007. 129(1-3): p. 51-65.
38. Santhosh, C., et al., *$CoFe_2O_4$ and $NiFe_2O_4$@graphene adsorbents for heavy metal ions – kinetic and thermodynamic analysis.* RSC Advances, 2015. 5(37): p. 28965-28972.
39. Li, Q., et al., *Preparation of Ag-$MnFe_2O_4$-bentonite Magnetic Composite for Pb(II)/Cd(II) Adsorption Removal and Bacterial Inactivation in Wastewater.* Chemical Research in Chinese Universities, 2018. 34: p. 1-9.
40. Zhang, T., et al., *Removal of heavy metals and dyes by clay-based adsorbents: From natural clays to 1D and 2D nano-composites.* Chemical Engineering Journal, 2020: p. 127574.
41. Yadav, Y., R. Gothalwal, and R.K. Tenguriya, *Management of Heavy Metal Pollution by using Bacterial Biomass.* International Journal of Biotech Trends and Technology (IJBTT), 2018. 8: p. 15-27.
42. Otunola, B.O. and O.O. Ololade, *A review on the application of clay minerals as heavy metal adsorbents for remediation purposes.* Environmental Technology & Innovation, 2020. 18: p. 100692.
43. Naushad, M. and Z.A. Al-Othman, *A book on ion exchange, adsorption and solvent extraction*. 2013: Nova Science Publishers, Incorporated.

44. Ruthven, D.M., *Principles of adsorption and adsorption processes*. 1984: John Wiley & Sons.
45. Abukhadra, M.R., et al., *Facile conversion of kaolinite into clay nanotubes (KNTs) of enhanced adsorption properties for toxic heavy metals (Zn^{2+}, Cd^{2+}, Pb^{2+}, and Cr^{6+}) from water*. J Hazard Mater, 2019. 374: p. 296-308.
46. Stirk, W.A. and J. van Staden, *Some physical factors affecting adsorption of heavy metals from solution by dried brown seaweed material.* South African Journal of Botany, 2001. 67(4): p. 615-619.
47. Usman, A.R.A., Y. Kuzyakov, and K. Stahr, *Effect of clay minerals on extractability of heavy metals and sewage sludge mineralization in soil.* Chemistry and Ecology, 2004. 20(2): p. 123-135.
48. AjayKumar, A.V., N.A. Darwish, and N. Hilal, *Study of various parameters in the biosorption of heavy metals on activated sludge.* World applied sciences journal, 2009. 5(5): p. 32-40.
49. Arora, R., *Adsorption of Heavy Metals–A Review.* Materials Today: Proceedings, 2019. 18: p. 4745-4750.
50. Jiang, M.-q., et al., *Adsorption of Pb(II), Cd(II), Ni(II) and Cu(II) onto natural kaolinite clay*. Desalination, 2010. 252(1-3): p. 33-39.
51. Es-sahbany, H., et al., *Adsorption of heavy metal (Cadmium) in synthetic wastewater by the natural clay as a potential adsorbent (Tangier-Tetouan-Al Hoceima–Morocco region).* Materials Today: Proceedings, 2021.
52. Southichak, B., et al., *Control Parameters Influencing the Adsorption of Heavy Metals by Protonated Reed Biomass.* Japanese Journal of Water Treatment Biology, 2007. 43(3): p. 159-167.
53. Qiu, W., et al., *Efficient removal of Cr(VI) by magnetically separable $CoFe_2O_4$/activated carbon composite.* Journal of Alloys and Compounds, 2016. 678: p. 179-184.
54. Mustapha, S., et al., *Potential of using kaolin as a natural adsorbent for the removal of pollutants from tannery wastewater*. Heliyon, 2019. 5(11): p. e02923.

55. Farhan, S.N. and A.A. Khadom, *Biosorption of heavy metals from aqueous solutions by Saccharomyces Cerevisiae.* International journal of industrial chemistry, 2015. 6(2): p. 119-130.
56. Müller, B.R., *Effect of particle size and surface area on the adsorption of albumin-bonded bilirubin on activated carbon.* Carbon, 2010. 48(12): p. 3607-3615.
57. Alhashimi, H.A. and C.B. Aktas, *Life cycle environmental and economic performance of biochar compared with activated carbon: a meta-analysis.* Resources, Conservation and Recycling, 2017. 118: p. 13-26.
58. Uddin, M.K., *A review on the adsorption of heavy metals by clay minerals, with special focus on the past decade.* Chemical Engineering Journal, 2017. 308: p. 438-462.
59. Mukherjee, S., *The science of clays.* Applications in Industry, Engineering and Environment, 2013.
60. Guggenheim, S., et al., *Introduction to the properties of clay minerals.* Teaching Mineralogy (Eds: Brady, J. B, DW Mogk, D. Perkins). Mineralogical Society of America. Washington, DC, 1997: p. 371-388.
61. Varga, G., *The structure of kaolinite and metakaolinite.* Epitoanyag, 2007. 59(1): p. 6-9.
62. Jaradat, K., et al., *Heating-freezing effects on the orientation of kaolin clay particles.* Applied Clay Science, 2017. 150: p. 163–174.
63. N J, V., *Pore architecture modulated clays and zeolites as solid acid catalysts for selected organic reactions*. 2015.
64. Krupskaya, V., et al., *Experimental Study of Montmorillonite Structure and Transformation of Its Properties under Treatment with Inorganic Acid Solutions.* Minerals, 2017. 7(4): p. 49.
65. Staunton, S. and M. Roubaud, *Adsorption of 137Cs on montmorillonite and illite: effect of charge compensating cation, ionic strength, concentration of Cs, K and fulvic acid.* Clays and clay minerals, 1997. 45(2): p. 251-260.
66. Unuabonah, E.I., et al., *Adsorption of Pb (II) and Cd (II) from aqueous solutions onto sodium tetraborate-modified Kaolinite clay: Equilibrium and thermodynamic studies.* Hydrometallurgy, 2008. 93(1-2): p. 1-9.

67. Chen, P., et al., *Adsorption of dodecylamine hydrochloride on graphene oxide in water.* Results in physics, 2017. 7: p. 2281-2288.
68. Na, P., et al., *Arsenic adsorption on Ti-pillared montmorillonite.* Journal of Chemical Technology & Biotechnology, 2010. 85(5): p. 708-714.
69. Ghorbanzadeh, N., et al., *Removal of arsenate and arsenite from aqueous solution by adsorption on clay minerals.* Geosystem Engineering, 2015. 18(6): p. 302-311.
70. Alshameri, A., et al., *Understanding the role of natural clay minerals as effective adsorbents and alternative source of rare earth elements: Adsorption operative parameters.* Hydrometallurgy, 2019. 185: p. 149-161.
71. Kurnosov, D., A. Burakov, and I. Burakova, *Development of a Bentonite Clay/Carbon Nanotubes Composite for Liquid-Phase Adsorption.* Materials Today: Proceedings, 2019. 11: p. 398-403.
72. Kakaei, S., et al., *Heavy metal removing by modified bentonite and study of catalytic activity.* Journal of Molecular Structure, 2020. 1199: p. 126989.
73. Abukhadra, M.R., et al., *Facile conversion of kaolinite into clay nanotubes (KNTs) of enhanced adsorption properties for toxic heavy metals (Zn^{2+}, Cd^{2+}, Pb^{2+}, and Cr^{6+}) from water.* Journal of Hazardous Materials, 2019. 374: p. 296-308.
74. Dim, P.E., et al., *Adsorption of chromium (VI) and iron (III) ions onto acid-modified kaolinite: Isotherm, kinetics and thermodynamics studies.* Arabian Journal of Chemistry, 2021. 14(4): p. 103064.
75. Bhattacharyya, K.G. and S.S. Gupta, *Adsorption of Fe(III), Co(II) and Ni(II) on ZrO–kaolinite and ZrO–montmorillonite surfaces in aqueous medium.* Colloids and Surfaces A: Physicochemical and Engineering Aspects, 2008. 317(1): p. 71-79.
76. Sari, A. and M. Tuzen, *Cd(II) adsorption from aqueous solution by raw and modified kaolinite.* Applied Clay Science, 2014. 88-89: p. 63-72.
77. Unuabonah, E.I., et al., *Adsorption of Pb (II) and Cd (II) from aqueous solutions onto sodium tetraborate-modified Kaolinite clay: Equilibrium and thermodynamic studies.* Hydrometallurgy, 2008. 93(1): p. 1-9.
78. Chu, Y., et al., *Synthesis and micro-mechanistic studies of histidine modified montmorillonite for lead(II) and copper(II) adsorption from wastewater.* Chemical Engineering Research and Design, 2020. 157: p. 142-152.

79. Chen, Y., et al., *Adsorption of Pb(II) by tourmaline-montmorillonite composite in aqueous phase.* Journal of Colloid and Interface Science, 2020. 575: p. 367-376.

80. Tohdee, K., L. Kaewsichan, and Asadullah, *Enhancement of adsorption efficiency of heavy metal Cu(II) and Zn(II) onto cationic surfactant modified bentonite.* Journal of Environmental Chemical Engineering, 2018. 6(2): p. 2821-2828.

81. Pawar, R.R., et al., *Use of activated bentonite-alginate composite beads for efficient removal of toxic Cu^{2+} and Pb^{2+} ions from aquatic environment.* Int J Biol Macromol, 2020.

82. Vazquez-Olmos, A.R., et al., *Mechanosynthesis of MFe_2O_4 (M = Co, Ni, and Zn) Magnetic Nanoparticles for Pb Removal from Aqueous Solution.* Journal of Nanomaterials, 2016. 2016: p. 9182024.

83. Aghrich, K., et al., *Experimental and first-principles study of the origin of the magnetic properties of $CoFe_2O_4$ spinel ferrite.* Applied Physics A, 2020. 126.

84. Qi, G., et al., *Preparation of $CoFe_2O_4$ nanoparticles based on high-gravity technology and application for the removal of lead.* Chemical Engineering Research and Design, 2019. 147: p. 520-528.

85. Wu, D., et al., *Phosphorylated chitosan/$CoFe_2O_4$ composite for the efficient removal of Pb(II) and Cd(II) from aqueous solution: Adsorption performance and mechanism studies.* Journal of Molecular Liquids, 2019. 277: p. 181-188.

86. Zhou, G., et al., *Synthesis of amino-functionalized bentonite/$CoFe_2O_4$@MnO_2 magnetic recoverable nanoparticles for aqueous Cd^{2+} removal.* Science of The Total Environment, 2019. 682: p. 505-513.

87. Culita, D.C., et al., *Effect of surfactant concentration on textural, morphological and magnetic properties of $CoFe_2O_4$ nanoparticles and evaluation of their adsorptive capacity for Pb(II) ions.* Ceramics International, 2015. 41(10, Part A): p. 13553-13560.

88. Xiao, Y., et al., *Synthesis and adsorption behavior of chitosan-coated $MnFe_2O_4$ nanoparticles for trace heavy metal ions removal.* Applied Surface Science, 2013. 285: p. 498-504.

89. Xu, W., et al., *Novel ternary nanohybrids of tetraethylenepentamine and graphene oxide decorated with $MnFe_2O_4$ magnetic nanoparticles for the adsorption of Pb(II).* Journal of Hazardous Materials, 2018. 358: p. 337-345.

90. Podder, M.S. and C.B. Majumder, *Bacteria immobilization on neem leaves/$MnFe_2O_4$ composite surface for removal of As(III) and As(V) from wastewater.* Arabian Journal of Chemistry, 2019. 12(8): p. 3263-3288.
91. Ma, J., et al., *A superparamagnetic $ZnFe_2O_4$@NH_2-SiO_2@PMDI@ dithizone microspheres as an effective selective adsorbent for Pb^{2+} from wastewater.* Journal of Environmental Chemical Engineering, 2019. 7(1): p. 102874.
92. Kuai, S., Z. Zhang, and Z. Nan, *Synthesis of Ce^{3+} doped $ZnFe_2O_4$ self-assembled clusters and adsorption of chromium (VI).* Journal of hazardous materials, 2013. 250: p. 229-237.
93. Desalegn, Y.M., D.M. Andoshe, and T.D. Desissa, *Composite of bentonite/$CoFe_2O_4$/hydroxyapatite for adsorption of Pb (II).* Materials Research Express, 2020. 7(11): p. 115501.
94. Hokkanen, S., et al., *Removal of Cd^{2+}, Ni^{2+} and $PO4^{3-}$ from aqueous solution by hydroxyapatite-bentonite clay-nanocellulose composite.* Int J Biol Macromol, 2018. 118(Pt A): p. 903-912.
95. Ahmad, I., F. Ali, and F. Rahim, *Clay Based Nanocomposites and Their Environmental Applications.* Nanomaterials for Environmental Applications and their Fascinating Attributes, 2018. 2: p. 166.
96. Thangavel, S. and G. Venugopal, *Understanding the adsorption property of graphene-oxide with different degrees of oxidation levels.* Powder technology, 2014. 257: p. 141-148.
97. Georgakilas, V., et al., *Functionalization of graphene: covalent and non-covalent approaches, derivatives and applications.* Chemical reviews, 2012. 112(11): p. 6156-6214.
98. Peng, W., et al., *Adsorption of methylene blue on graphene oxide prepared from amorphous graphite: Effects of pH and foreign ions.* Journal of Molecular Liquids, 2016. 221: p. 82-87.
99. Sitko, R., et al., *Adsorption of divalent metal ions from aqueous solutions using graphene oxide.* Dalton transactions, 2013. 42(16): p. 5682-5689.

100. Dastgheib, S.A. and D.A. Rockstraw, *A model for the adsorption of single metal ion solutes in aqueous solution onto activated carbon produced from pecan shells.* Carbon, 2002. 40(11): p. 1843-1851.
101. Peng, W., et al., *A review on heavy metal ions adsorption from water by graphene oxide and its composites.* Journal of Molecular Liquids, 2017. 230: p. 496-504.
102. Gopalakrishnan, A., et al., *Removal of heavy metal ions from pharma-effluents using graphene-oxide nanosorbents and study of their adsorption kinetics.* Journal of Industrial and Engineering Chemistry, 2015. 30: p. 14-19.
103. Wu, W., et al., *Highly efficient removal of Cu (II) from aqueous solution by using graphene oxide.* Water, Air, & Soil Pollution, 2013. 224(1): p. 1-8.
104. Madadrang, C.J., et al., *Adsorption behavior of EDTA-graphene oxide for Pb (II) removal.* ACS applied materials & interfaces, 2012. 4(3): p. 1186-1193.
105. Peng, W., et al., *Comparison of Pb (II) adsorption onto graphene oxide prepared from natural graphites: Diagramming the Pb (II) adsorption sites.* Applied Surface Science, 2016. 364: p. 620-627.
106. Melikoğlu, A.Y., S.E. Bilek, and S. Cesur, *Optimum alkaline treatment parameters for the extraction of cellulose and production of cellulose nanocrystals from apple pomace.* Carbohydrate polymers, 2019. 215: p. 330-337.
107. Veeramachineni, A.K., et al., *Optimizing extraction of cellulose and synthesizing pharmaceutical grade carboxymethyl sago cellulose from Malaysian sago pulp.* Applied Sciences, 2016. 6(6): p. 170.
108. Marcano, D.C., et al., *Improved synthesis of graphene oxide.* ACS nano, 2010. 4(8): p. 4806-4814.
109. Fu, Y. and X. Wang, *Magnetically separable $ZnFe_2O_4$–graphene catalyst and its high photocatalytic performance under visible light irradiation.* Industrial & engineering chemistry research, 2011. 50(12): p. 7210-7218.
110. Tul Ain, Q., et al., *The systemic effect of PEG-nGO-induced oxidative stress in vivo in a rodent model.* Beilstein Journal of Nanotechnology, 2019. 10: p. 901-911.
111. Zawrah, M., et al., *Characterization of Sol-gel Fabricated Cobalt Ferrite $CoFe_2O_4$ Nanoparticles.* 2018.

112. Zong, M., et al., *One-pot hydrothermal synthesis of RGO/$CoFe_2O_4$ composite and its excellent microwave absorption properties.* Materials Letters, 2014. 114: p. 52-55.
113. Zen, S., et al., *Activated kaolin's potential adsorbents for the removal of Derma Blue R67 acid dye: kinetic and thermodynamic studies.* Desalination and Water Treatment, 2018. 112: p. 196-206.
114. Olusegun, S.J. and N.D.S. Mohallem, *Comparative adsorption mechanism of doxycycline and Congo red using synthesized kaolinite supported $CoFe_2O_4$ nanoparticles.* Environ Pollut, 2020. 260: p. 114019.
115. Wang, W., et al., *One-pot hydrothermal synthesis of reduced graphene oxide/zinc ferrite nanohybrids and its catalytic activity on the thermal decomposition of ammonium perchlorate.* Journal of Saudi Chemical Society, 2019. 23(2): p. 133-140.
116. Li, J., et al., *One-pot in situ synthesis of a $CoFe_2O_4$ nanoparticle-reduced graphene oxide nanocomposite with high performance for levodopa sensing.* RSC advances, 2015. 5(121): p. 99669-99677.
117. Mustapha, S., et al., *Potential of using kaolin as a natural adsorbent for the removal of pollutants from tannery wastewater*. Heliyon, 2019. 5(11): p. e02923.
118. Huang, X., et al., *Preparation of a Three-Dimensional Porous Graphene Oxide–Kaolinite–Poly (vinyl alcohol) Composite for Efficient Adsorption and Removal of Ciprofloxacin.* Langmuir, 2020. 36(37): p. 10895-10904.
119. Foroutan, R., et al., *Performance of montmorillonite/graphene oxide/$CoFe_2O_4$ as a magnetic and recyclable nanocomposite for cleaning methyl violet dye-laden wastewater.* Advanced Powder Technology, 2020. 31(9): p. 3993-4004.
120. Romero-Guerrero, L., et al., *Chemical, Mineralogical, and Refractory Characterization of Kaolin in the Regions of Huayacocotla-Alumbres, Mexico.* Advances in Materials Science and Engineering, 2018. 2018.
121. Sumathi, S. and V.S. Kirankumar, *Catalytic and electrical study of substituted cobalt ferrite*. 2016.
122. Lertcumfu, N., et al., *Influence of graphene oxide additive on physical, microstructure, adsorption, and photocatalytic properties of calcined kaolinite-based geopolymer ceramic composites.* Colloids And Surfaces A: Physicochemical And Engineering Aspects, 2020. 602: p. 125080.

123. Wang, D., et al., *Synthesis of a multifunctional graphene oxide-based magnetic nanocomposite for efficient removal of Cr (VI).* Langmuir, 2017. 33(28): p. 7007-7014.
124. He, K., et al., *Enhanced removal performance for methylene blue by kaolin with graphene oxide modification.* Journal of the Taiwan Institute of Chemical Engineers, 2018. 89: p. 77-85.
125. Foroutan, R., et al., *Performance of algal activated carbon/Fe_3O_4 magnetic composite for cationic dyes removal from aqueous solutions.* Algal Research, 2019. 40: p. 101509.
126. Elass, K., et al., *Removal of methyl violet from aqueous solution using a stevensite-rich clay from Morocco.* Applied Clay Science, 2011. 54(1): p. 90-96.
127. Naeem, H., et al., *Facile synthesis of graphene oxide–silver nanocomposite for decontamination of water from multiple pollutants by adsorption, catalysis and antibacterial activity.* Journal of environmental management, 2019. 230: p. 199-211.
128. Saleh, T.A., A. Sarı, and M. Tuzen, *Chitosan-modified vermiculite for As (III) adsorption from aqueous solution: equilibrium, thermodynamic and kinetic studies.* Journal of Molecular Liquids, 2016. 219: p. 937-945.
129. Shukla, S. and G. Kisku, *Linear and non-linear kinetic modeling for adsorption of disperse dye in batch process.* Research journal of environmental toxicology, 2015. 9(6): p. 320.
130. Xu, H., et al., *Removal of lead (II) and cadmium (II) from aqueous solutions using spent Agaricus bisporus.* The Canadian Journal of Chemical Engineering, 2013. 91(3): p. 421-431.
131. Li, H., et al., *Removal of tannin from aqueous solution by adsorption onto treated coal fly ash: kinetic, equilibrium, and thermodynamic studies.* Industrial & Engineering Chemistry Research, 2013. 52(45): p. 15923-15931.
132. Foroutan, R., et al., *Application of nano-silica particles generated from offshore white sandstone for cadmium ions elimination from aqueous media.* Environmental Technology & Innovation, 2020. 19: p. 101031.